

Dear author,

Please note that changes made in the online proofing system will be added to the article before publication but are not reflected in this PDF.

We also ask that this file not be used for submitting corrections.



The isotope effect of nitrate assimilation in the Antarctic Zone: Improved estimates and paleoceanographic implications

François Fripiat^{a,*}, Alfredo Martínez-García^a, Sarah E. Fawcett^b
Preston C. Kemeny^{c,d}, Anja S. Studer^a, Sandi M. Smart^e, Florian Rubach^a
Sergey Oleynik^d, Daniel M. Sigman^d, Gerald H. Haug^a

^a Max Planck Institute for Chemistry, Mainz, Germany

^b Department of Oceanography, University of Cape Town, Rondebosch, South Africa

^c Division of Geological and Planetary Sciences, California Institute of Technology, Pasadena, California, USA

^d Department of Geosciences, Princeton University, Princeton, New Jersey, USA

^e Department of Earth Sciences, Stellenbosch University, Matieland, Stellenbosch, South Africa

Received 11 June 2018; revised 28 November 2018; accepted in revised form 5 December 2018; available online xxxx

Abstract

Both the nitrogen (N) isotopic composition ($\delta^{15}\text{N}$) of the nitrate source and the magnitude of isotope discrimination associated with nitrate assimilation are required to estimate the degree of past nitrate consumption from the $\delta^{15}\text{N}$ of organic matter in Southern Ocean sediments (e.g., preserved within diatom microfossils). It has been suggested that the amplitude of isotope discrimination (i.e. the isotope effect) correlates with mixed layer depth, driven by a physiological response of phytoplankton to light availability, which introduces complexity to the interpretation of sedimentary records. However, most of the isotope effect estimates that underpin this hypothesis derive from acid-preserved water samples, from which nitrite would have been volatilized and lost during storage. Nitrite $\delta^{15}\text{N}$ in Antarctic Zone surface waters is extremely low ($-61 \pm 20\text{‰}$), consistent with the expression of an equilibrium isotope effect associated with nitrate–nitrite interconversion. Its loss from the combined nitrate+nitrite pool would act to raise the $\delta^{15}\text{N}$ of nitrate, potentially yielding overestimation of the isotope effect. Here, we revisit the nitrate assimilation isotope effect in the Antarctic Zone with measurements of the $\delta^{15}\text{N}$ and concentration of nitrate with and without nitrite, using frozen sea water samples from 5 different cruises that collectively cover all sectors of the Southern Ocean. The N isotope effect estimated using nitrate+nitrite $\delta^{15}\text{N}$ is relatively constant ($5.5 \pm 0.6\text{‰}$) across the Antarctic Zone, shows no relationship with mixed layer depth, and is in agreement with sediment trap $\delta^{15}\text{N}$ measurements. Estimates of the N isotope effect derived from nitrate-only $\delta^{15}\text{N}$ are higher and more variable ($7.9 \pm 1.5\text{‰}$), consistent with an artifact from nitrate–nitrite isotope exchange. In the case of the Southern Ocean, we conclude that the $\delta^{15}\text{N}$ of nitrate+nitrite better reflects the isotope effect of nitrate assimilation. The stability of this isotope effect across the Antarctic Zone simplifies the effort to reconstruct past degree of nitrate consumption.

© 2018 Elsevier Ltd. All rights reserved.

1. INTRODUCTION

In the Southern Ocean and especially south of the Polar Front (i.e. the Antarctic Zone), deep nutrient-rich waters rise to the surface and are returned to the subsurface before nitrate and phosphate are fully used by phytoplankton. The

* Corresponding author.

E-mail address: f.fripiat@mpic.de (F. Fripiat).

ineffectiveness of phytoplankton at drawing down major nutrients in Southern Ocean surface waters has been attributed to co-limitation by iron and light (Martin et al., 1990; Mitchel et al., 1991) and allows (i) CO₂ sequestered in the deep ocean to be released to the atmosphere (Sigman et al., 2010) and (ii) the unused nutrient pool in the surface waters of the Southern Ocean to be exported to the low latitudes (Sarmiento et al., 2004; Palter et al., 2010).

Nitrate (NO₃⁻) assimilation by phytoplankton preferentially incorporates ¹⁴N into new biomass, leaving the residual NO₃⁻ pool enriched in ¹⁵N (Wada and Hattori, 1978; Montoya and McCarthy, 1995; Granger et al., 2004, 2010). The kinetic isotope effect (ε) expresses the degree of isotope discrimination, and is commonly defined as the ratio of reaction rates at which the two isotopes are converted from reactant to product (i.e. ε (‰) = ((1 - ¹⁵k/¹⁴k) × 1000); where ^xk is the rate constant for the ^xN-containing reactant). The isotopic fractionation of NO₃⁻ assimilation links the degree of NO₃⁻ consumption to the δ¹⁵N (= ((¹⁵N/¹⁴N)_{sample} / (¹⁵N/¹⁴N)_{reference} - 1) × 1000, with atmospheric N₂ as the reference) of both the NO₃⁻ and the newly produced organic matter (Altabet and Francois, 1994a,b; Sigman et al., 1999a). Thus, the δ¹⁵N of fossil-bound organic matter recovered from Southern Ocean sediment cores provides a measure of the degree of nitrate consumption in the past and has been used to investigate possible mechanisms for driving the changes in atmospheric CO₂ observed over glacial cycles (Robinson and Sigman, 2008; Martinez-Garcia et al., 2014; Studer et al., 2015; Wang et al., 2017).

During at least the last two ice ages, the δ¹⁵N of diatom- and deep-sea coral-bound organic N in Antarctic sediments was ~4‰ higher than it is today (Studer et al., 2015; Wang et al., 2017), indicative of an enhanced degree of nitrate consumption during the ice ages. Together with the observed glacial decrease in Antarctic productivity (Kohfeld et al., 2005; Jaccard et al., 2013), this implies that the supply of NO₃⁻ to Antarctic Zone surface waters was significantly reduced during the ice ages, leading to the hypothesis of Antarctic “stratification” as one of the dominant drivers of glacial-interglacial variation in atmospheric pCO₂ (Francois et al., 1997; Sigman et al., 2010).

The δ¹⁵N of the NO₃⁻ supply and the isotope effect of NO₃⁻ assimilation are two key parameters required for estimating the degree of past NO₃⁻ consumption. Previous studies in the Southern Ocean have suggested systematic variations in the isotope effect with mixed layer depth that would have implications for the δ¹⁵N of sinking particulate N (PN) and fossil-bound N under changing environmental conditions (DiFiore et al., 2010). However, most of these measurements were made on acidified water samples, from which nitrite (NO₂⁻) would have been largely lost during storage, due to the volatility of HNO₂ followed by its rapid conversion into gaseous nitrogen oxide (NO and NO₂) (Park and Lee, 1988; Rayson et al., 2012). NO₂⁻ can be reliably removed prior to isotope analysis through the addition of sulfamic acid or sulfanilamide, allowing the measurement of both NO₃⁻ + NO₂⁻ and NO₃⁻-only δ¹⁵N and δ¹⁸O for seawater samples stored frozen since collection (Granger and Sigman, 2009; Weigand et al., 2016). In

late-summer water column profiles, Kemeny et al. (2016) reported a systematic difference between NO₃⁻ + NO₂⁻ δ¹⁵N and NO₃⁻ δ¹⁵N in Antarctic Zone surface waters, with NO₃⁻ δ¹⁵N typically being 0.5–1.0‰ higher than NO₃⁻ + NO₂⁻ δ¹⁵N. They suggested that NO₃⁻–NO₂⁻ interconversion occurs in the euphotic zone, leading to the expression of an N equilibrium isotope effect between NO₃⁻ and NO₂⁻, enriching NO₃⁻ and depleting NO₂⁻ in ¹⁵N. Seasonal mixed layer deepening was suggested to entrain nitrite oxidizers from the subsurface into the late-summer mixed layer, discouraging NO₂⁻ oxidation due to light inhibition and favoring the reversibility of the nitrite oxidoreductase (NXR) enzyme.

In this study, we revisit the mean value and variability of the isotope effect of NO₃⁻ assimilation in the Antarctic Zone using isotopic data from seawater samples that were stored frozen and not acidified, thus avoiding potential artifacts from the coupling of putative NO₃⁻–NO₂⁻ interconversion with subsequent NO₂⁻ loss during storage.

2. MATERIALS AND METHODS

2.1. Background: hydrography

We draw a distinction between the Polar Antarctic Zone (PAZ), the area south of the Southern Antarctic Circumpolar Current Front (SACCF), and the Open Antarctic Zone (OAZ), the area between the SACCF and the Polar Front

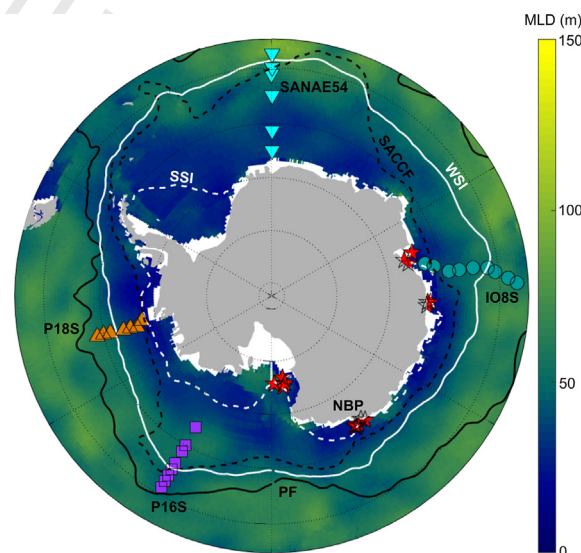


Fig. 1. Location of the stations (symbols) overlaid on mixed layer depth (MLD) climatology for February (Pellichero et al., 2017). The Polar Front (PF) and the Southern Antarctic Circumpolar Current Front (SACCF) according to Orsi et al. (1995) are indicated by the dashed and solid black lines, respectively. The solid and dashed white lines represent the mean winter maximal (WSI) and summer minimal (SSI) sea ice extent (1979–2008, ≥ 15% ice cover) (Raymond, 2014). The cyan inverted triangles indicate the stations for SANA E54, the orange triangles for P18S, the purple squares for P16S (Kemeny et al., 2016), the blue-green circles for IO8S, and the red stars for the NBP cruises (NBP01-1 and NBP06-8) (DiFiore et al., 2009).

(Fig. 1) (e.g., Sigman et al., 2009a). The boundary between these two zones is also roughly delineated by either the northernmost extent of winter sea-ice or the southernmost extent of Upper Circumpolar Deep Water (UCDW) (Orsi et al., 1995).

Across the Antarctic Zone, NO_3^- is supplied by Ekman pumping and vertical mixing across the base of the winter mixed layer. Nutrient-rich Circumpolar Deep Water (CDW) upwells in the Antarctic Zone. Part of the upwelled CDW gains buoyancy due to warming and freshening, causing it to flow northward in the Ekman layer, ultimately sinking north of the Polar Front into the main oceanic pycnocline. The remainder loses buoyancy near Antarctica, inducing deep convection over the continental shelves and leading to Antarctic Bottom Water (AABW) formation (Fig. 2). Deep ventilation may also occur in the Antarctic Zone away from the coasts, for example, due to mixing by mesoscale eddies (Abernathy and Ferreira, 2015).

In summer, the upper halocline layer in most of the Antarctic Zone (hereafter referred as Antarctic Surface Water, AASW) is characterized by both a relatively fresh, well-mixed surface layer, and a subsurface temperature minimum (T_{\min}) layer below (Fig. 2c and A1c; hereafter referred to as the ‘ T_{\min} ’ stations) (e.g., Park et al., 1998). The latter is also known as “Winter Water” because it is the remnant of the previous winter mixed layer that has become isolated in the shallow subsurface by spring-summer warming and freshening of the overlying water. AASW tends to be thicker in the OAZ due to higher wind stress and thus deeper vertical mixing near the Polar Front, with generally shallower mixed layers in the seasonally sea-ice covered areas to the south (Fig. 1) (Pellichero et al., 2017). Near and above the continental shelves (hereafter referred as to the ‘margin’ stations), a shallow mixed layer usually caps a relatively homogeneous, dense, near-freezing shelf water mass. The latter has undergone a brine rejection-driven increase in salinity, a prerequisite for the formation of AABW (e.g., Orsi et al., 1999). As a result

of lateral exchange, intrusion of AASW and CDW southward toward the continental shelves can generate a distinct subsurface temperature maximum between the summertime mixed layer and the shelf waters below (hereafter referred to as the ‘ T_{\max} ’ stations) (e.g., DiFiore et al., 2009).

2.2. Sample collection

New and previously published $\text{NO}_3^- + \text{NO}_2^-$ and NO_3^- -only $\delta^{15}\text{N}$ and $\delta^{18}\text{O}$ measurements are reported from the Atlantic, Indian, and Pacific sectors of the Antarctic Zone (Fig. 1 and Table 1). New hydrographic sections are GOSHIP IO8S (February 2016) in the eastern Indian sector, P18S (January 2017) in the eastern Pacific sector, and SANAE54 (December-January 2014–2015) in the Atlantic sector along the Greenwich Meridian. These new datasets are compiled in combination with previous measurements located near the Antarctic continent (DiFiore et al., 2009; NBP cruises) and in the western Pacific sector (Kemeny et al., 2016; GOSHIP P16S transect).

A total of 50 hydrocasts (24 unpublished) were collected between the Antarctic continental shelf and the Polar Front. Most of the hydrocasts ($n=46$) were collected between December 12th and April 9th during the various years (Table 1). This summer-early fall condition captures the major extent of annual NO_3^- depletion in the mixed layer. Four hydrocasts from the Ross Sea (NBP01-01) were sampled in November at the onset of the growing period (DiFiore et al., 2009). Unfiltered water samples were collected and immediately frozen (-20°C) until their analysis at home-based laboratories (Max Planck Institute for Chemistry (MPIC) for IO8S and P18S and Princeton University for SANAE54).

2.3. Nitrate isotope analysis

$\text{NO}_3^- + \text{NO}_2^-$ $\delta^{15}\text{N}$ and $\delta^{18}\text{O}$ were determined using the denitrifier method (Sigman et al., 2001; Casciotti et al.,

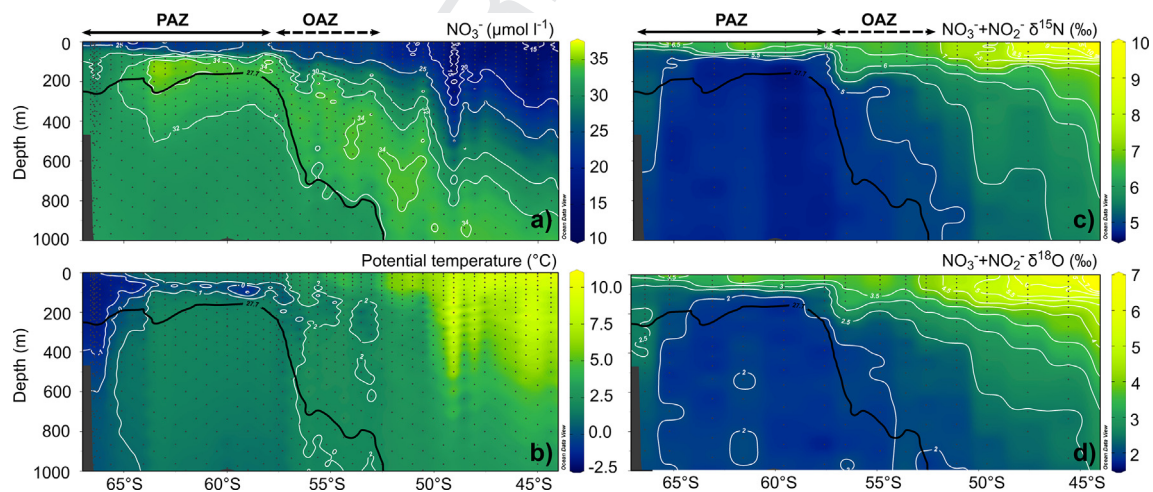


Fig. 2. Meridional depth sections of NO_3^- concentration (a), potential temperature (b), $\text{NO}_3^- + \text{NO}_2^-$ $\delta^{15}\text{N}$ (c) and $\text{NO}_3^- + \text{NO}_2^-$ $\delta^{18}\text{O}$ (d) in the Indian Sector at 78–95°E (IO8S). The thin white lines are contours of NO_3^- concentration (a), potential temperature (b), $\text{NO}_3^- + \text{NO}_2^-$ $\delta^{15}\text{N}$ (c) and $\text{NO}_3^- + \text{NO}_2^-$ $\delta^{18}\text{O}$ (d). The isopycnal delimiting Upper and Lower Circumpolar Deep Water is indicated with the thick black solid line. The sections were generated with Ocean Data View [Available at <http://odv.awi.de>].

Table 1

Averages (\pm sd) for the isotope effects estimated by pooling different datasets (Eq. (4)). The “AASW average” isotope effects are calculated using the entire AASW dataset. “Regional average” isotope effects are calculated using data from individual cruises (IO8S, P16S, P18S, and SANAE54) or from the distinct regional continental shelf settings of the NBP cruises (Dumont D’Urville Sea, Davis Sea, Prydz Bay, and Ross Sea). “Station average” isotope effects are estimated by first calculating the isotope effect for each station and then the average for each cruise or regional setting.

Cruise Name (Sector)	Location	Date	PAZ #	OAZ #	Regional ϵ average (‰)				Station ϵ average ^c (‰)			
					$\text{NO}_3^- + \text{NO}_2^-$		NO_3^- -only		$\text{NO}_3^- + \text{NO}_2^-$		NO_3^- -only	
					$^{15}\epsilon$	$^{18}\epsilon$	$^{15}\epsilon$	$^{18}\epsilon$	$^{15}\epsilon$	$^{18}\epsilon$	$^{15}\epsilon$	$^{18}\epsilon$
IO8 (Indian)	83°E	Feb. 2016	6	3	5.9 \pm 0.4	4.4 \pm 0.3	7.6 \pm 0.6	4.2 \pm 0.3	6.1 \pm 0.5	4.3 \pm 0.8	8.0 \pm 0.6	4.5 \pm 1.0
P16 (Pacific) ^a	150°W	Apr. 2014	6	2	4.9 \pm 0.3	4.6 \pm 0.3	6.7 \pm 0.5	4.5 \pm 0.3	5.3 \pm 0.9	4.2 \pm 0.9	8.4 \pm 2.2	4.0 \pm 0.7
P18 (Pacific)	103°W	Jan. 2017	2	5	5.8 \pm 0.5	4.8 \pm 0.5	8.4 \pm 0.7	4.2 \pm 0.5	6.1 \pm 1.6	3.5 \pm 1.0	10.8 \pm 3.0	3.3 \pm 1.4
SANAE54 (Atlantic)	0°W	Dec-Feb 2014–2015	7	1	4.8 \pm 0.3	4.3 \pm 0.2	6.2 \pm 0.2	4.8 \pm 0.3	4.5 \pm 1.3	4.3 \pm 0.8	6.4 \pm 1.1	5.2 \pm 1.7
NBP01-01 (DDU) ^{b,c}	146°E	Feb. 2001	6	0	3.2 \pm 0.4 ^d	1.9 \pm 0.9 ^d			5.7 \pm 2.7	5.9 \pm 4.6		
NBP01-01 (Davis Sea) ^c	93°E	Feb. 2001	3	0	4.9 \pm 0.4	4.8 \pm 0.8			4.9 \pm 0.9	4.7 \pm 1.6		
NBP01-01 (Prydz Bay) ^c	76°E	Mar. 2001	5	0	3.8 \pm 0.6 ^d	4.2 \pm 0.7 ^d			6.7 \pm 2.8	4.5 \pm 1.2		
NBP06-08 (Ross Sea) ^c	174°E	Nov. 2006	4	0	5.8 \pm 0.5	6.3 \pm 0.8			5.7 \pm 0.4	6.2 \pm 0.2		
AASW average			39	11	5.2 \pm 0.1	4.2 \pm 0.1	7.3 \pm 0.3	4.5 \pm 0.2	5.7 \pm 1.5	4.4 \pm 1.5	8.5 \pm 2.0	4.2 \pm 1.1
AASW average (without DDU and Ross Sea) ^d			29	11	5.4 \pm 0.2	4.6 \pm 0.1						

^a Kemeny et al. (2016).

^b Dumont D’Urville Sea.

^c DiFiore et al. (2009).

^d The variability in the AASW for these areas is close to the analytical precision.

^e Only the stations with a vertical isotopic gradient greater than 0.2‰ are used.

2002; Weigand et al., 2016). Briefly, 10–20 nmol of $\text{NO}_3^- + \text{NO}_2^-$ was quantitatively converted to N_2O gas by a strain of denitrifying bacteria (*Pseudomonas chlororaphis* f. sp. *aureofaciens* ATCC n°13985) that lacks an active N_2O reductase enzyme. In both laboratories, the isotopic composition of N_2O was measured by gas chromatography/isotope ratio mass spectrometry using a purpose-built online N_2O extraction and purification system and Thermo MAT 253 mass spectrometer (Weigand et al., 2016). Measurements are referenced to air N_2 for $\delta^{15}\text{N}$ and Vienna Standard Mean Ocean Water (VSMOW) for $\delta^{18}\text{O}$ using the NO_3^- reference materials IAEA-NO3, with a $\delta^{15}\text{N}$ of 4.7‰ and a $\delta^{18}\text{O}$ of 25.6‰, and USGS-34, with a $\delta^{15}\text{N}$ of -1.8‰ and a $\delta^{18}\text{O}$ of -27.9‰ (Böhlke et al., 2003).

During the reduction of NO_3^- and NO_2^- to N_2O by the denitrifier method, O atoms are either transferred to the resulting nitrogen oxide pool (ultimately to N_2O) or lost as water, and isotopic fractionation is known to occur during these branching reactions (Casciotti et al., 2002). For NO_3^- , this effect is accounted for by calibration with NO_3^- isotopic reference materials. Because NO_2^- reduction to N_2O represents a smaller fractional loss of oxygen atoms than NO_3^- reduction (3/4 vs. 5/6), the N_2O generated from NO_2^- by the denitrifier method is ~25‰ lower in $\delta^{18}\text{O}$ than N_2O generated from NO_3^- with the same initial $\delta^{18}\text{O}$ (Casciotti et al., 2007). This methodological bias is corrected for each sample by adding to $\text{NO}_3^- + \text{NO}_2^-$ $\delta^{18}\text{O}$ the product of 25‰ and the relative contribution of NO_2^- to $\text{NO}_3^- + \text{NO}_2^-$ (Kemeny et al., 2016). In order to isolate and measure the NO_3^- -only $\delta^{15}\text{N}$ and $\delta^{18}\text{O}$, samples with detectable NO_2^- concentrations were treated with sulfamic acid prior to NO_3^- isotope analysis (Granger and Sigman, 2009).

Replicate analyses (100% of the samples) at MPIC indicate median 1sd reproducibility of <0.07‰ and <0.13‰ for $\delta^{15}\text{N}$ and $\delta^{18}\text{O}$, respectively (i.e., similar to <0.05‰ and <0.14‰ for P16S and SANA54 analyzed at Princeton). There was no significant difference in reproducibility between samples treated with sulfamic acid and their untreated counterparts. Seawater samples from the deep North Atlantic (MPIC) and Pacific (Princeton University) were used as in-house standards and measured two to three times in each run, the long-term reproducibility was <0.08‰ and <0.12‰ for $\delta^{15}\text{N}$ and $\delta^{18}\text{O}$, respectively. In the case of the NBP samples, which were analyzed a decade earlier using the protocol and extraction system of Casciotti et al. (2002), the replicate analyses indicated a median 1sd reproducibility of 0.17‰ for $\delta^{15}\text{N}$ and 0.26‰ for $\delta^{18}\text{O}$ (DiFiore et al., 2009).

2.4. Estimating the isotope effect of nitrate assimilation

If NO_3^- assimilation proceeds with a constant isotope effect and if the reactant N pool (NO_3^-) is neither significantly replenished nor subject to any loss, then the isotopic evolution of the residual NO_3^- , instantaneous PN (hereafter indicated with the superscript “inst”), and accumulated PN (hereafter indicated with the superscript “acc”) are described by Rayleigh fractionation kinetics, with the following equations (Mariotti et al., 1981):

$$R_{\text{NO}_3^-} = R_{\text{NO}_3^-}^0 \cdot f^{-(10^{-3} \cdot \varepsilon)} \quad (1)$$

$$R_{\text{PN}}^{\text{inst}} = (1 - 10^{-3} \cdot \varepsilon) \cdot R_{\text{NO}_3^-} \quad (2)$$

$$R_{\text{PN}}^{\text{acc}} = R_{\text{NO}_3^-}^0 \cdot \frac{1 - f^{(1-10^{-3} \cdot \varepsilon)}}{1 - f} \quad (3)$$

where f is the fraction of NO_3^- remaining (i.e. $f = [\text{NO}_3^-] / [\text{NO}_3^-]_{\text{initial}}$), the superscript 0 is the initial condition, R is the $^{15}\text{N}/^{14}\text{N}$ or $^{18}\text{O}/^{16}\text{O}$ ratio, and ε is the isotope effect for either N or O isotopes. Since O atoms are not incorporated into biomass, only Eq. (1) is valid for the O isotopes. Because phytoplankton discriminate against ^{15}N and ^{18}O to the same extent during NO_3^- assimilation ($^{15}\varepsilon \approx ^{18}\varepsilon$; Granger et al., 2004, 2010; Karsh et al., 2012, 2014), the residual NO_3^- $\delta^{15}\text{N}$ and $\delta^{18}\text{O}$ rise equally if only assimilation is taking place in a water parcel. Eqs. (1)–(3) include the reasonable assumption that the abundances of both the ^{15}N and ^{18}O isotope are low, implying that $^{14}\text{N} \sim ^{14}\text{N} + ^{15}\text{N}$ and $^{16}\text{O} \sim ^{16}\text{O} + ^{17}\text{O} + ^{18}\text{O}$ (Mariotti et al., 1981). Rearranging Eq. (1) and using delta notation instead of the ratio allows us to formulate a linear relationship that has negative ε as its slope and initial conditions (NO_3^- concentration and $\delta^{15}\text{N}$) as intercept (Mariotti et al., 1981), as shown here for the N isotopes:

$$\begin{aligned} 10^3 \cdot \ln(10^{-3} \cdot \delta^{15}\text{N}_{\text{NO}_3^-} + 1) \\ = -\varepsilon \cdot \ln([\text{NO}_3^-]) \\ + \left(10^3 \cdot \ln(10^{-3} \cdot \delta^{15}\text{N}_{\text{NO}_3^-}^0 + 1) + \varepsilon \cdot \ln([\text{NO}_3^-]_0) \right) \end{aligned} \quad (4)$$

In logarithmic equations of the form $\ln[(1+u)/(1+v)]$, where u and v are real numbers that are small relative to 1, which is the case for most $10^{-3} \cdot \delta$ values, $\ln[(1+u)/(1+v)]$ can be approximated by $u - v$. Consequently, Eq. (4) can be simplified to give the following widely applied approximate equation (Mariotti et al., 1981):

$$\begin{aligned} \delta^{15}\text{N}_{\text{NO}_3^-} = -\varepsilon \cdot \ln([\text{NO}_3^-]) \\ + \left(\delta^{15}\text{N}_{\text{NO}_3^-}^0 + \varepsilon \cdot \ln([\text{NO}_3^-]_0) \right) \end{aligned} \quad (5)$$

We calculate a difference of less than ~0.1‰ between Eqs. (4) and (5) for estimates of the NO_3^- assimilation isotope effect in the Antarctic Zone. While Eq. (5) is useful for illustrating Rayleigh fractionation trends in the plotting spaces of NO_3^- $\delta^{15}\text{N}$ vs. $\ln([\text{NO}_3^-])$ and NO_3^- $\delta^{18}\text{O}$ vs. $\ln([\text{NO}_3^-])$, we use the more accurate Eq. (4) to estimate isotope effects.

3. RESULTS

3.1. Nitrite concentration and impact on isotope distribution

In all the Southern Ocean stations analyzed, there is a small but significant accumulation of NO_2^- near the surface, increasing from near-zero concentrations in deep water to ~0.25 $\mu\text{mol l}^{-1}$ (Fig. 3). This is in contrast to low-latitude areas, where a primary NO_2^- maximum is typically found at the base of the euphotic layer, with <0.02 $\mu\text{mol l}^{-1}$ in the surface mixed layer (Lomas and Lipschultz, 2006;

309 Fawcett et al., 2015; Peng et al., in press), but consistent
 310 with a recent compilation of observations for the high latitude
 311 ocean showing similarly elevated levels of NO_2^-
 312 throughout the mixed layer (Zakem et al., 2018). The
 313 removal of NO_2^- from samples with detectable NO_2^- concentrations
 314 has a significant impact on the nitrate isotope distribution (Figs. 4 and 5a).
 315 NO_3^- -only $\delta^{15}\text{N}$ is higher than $\text{NO}_3^- + \text{NO}_2^-$ $\delta^{15}\text{N}$ by $\sim 0.7 \pm 0.2\text{‰}$ in the summer
 316 surface mixed layer, but it is not significantly different deeper in
 317 the water column. In contrast, there is no clear difference
 318 ($0.0 \pm 0.2\text{‰}$) between NO_3^- -only and $\text{NO}_3^- + \text{NO}_2^-$ $\delta^{18}\text{O}$
 319 throughout the upper water column (Figs. 4 and 5b).
 320

3.2. Nitrate isotope distribution in the Antarctic Zone

322 The $\delta^{15}\text{N}$ and $\delta^{18}\text{O}$ of both NO_3^- -only and $\text{NO}_3^- + \text{NO}_2^-$
 323 increase toward the surface in concert with the upward
 324 decline in NO_3^- concentration, reflecting the preferential
 325 assimilation of ^{14}N - and ^{16}O -bearing NO_3^- by phytoplankton
 326 (Figs. 2 and 4). In the OAZ, $\text{NO}_3^- + \text{NO}_2^-$ $\delta^{15}\text{N}$
 327 increases from 5.0‰ in the deeper layers to 6.6‰ at the surface
 328 on average, and from 5.0‰ to 7.4‰ for NO_3^- -only
 329 $\delta^{15}\text{N}$. Both NO_3^- -only and $\text{NO}_3^- + \text{NO}_2^-$ $\delta^{18}\text{O}$ increase to
 330 the same extent across this depth interval, from 1.9‰ to
 331 3.7‰ on average. At the T_{\min} stations in the PAZ, $\text{NO}_3^- +$
 332 NO_2^- $\delta^{15}\text{N}$ increases from 4.8‰ to 6.2‰ on average, and
 333 from 4.8‰ to 6.9‰ for NO_3^- -only $\delta^{15}\text{N}$. Similar to the
 334 OAZ, both NO_3^- -only and $\text{NO}_3^- + \text{NO}_2^-$ $\delta^{18}\text{O}$ increase to
 335 the same extent, from 2.0‰ to 3.4‰. The northward
 336 increases in NO_3^- -only and $\text{NO}_3^- + \text{NO}_2^-$ $\delta^{15}\text{N}$ and $\delta^{18}\text{O}$
 337 result from progressive NO_3^- consumption during the
 338 Ekman transport of surface water from the Antarctic Zone
 339 to the Polar Frontal and Subantarctic Zones (Figs. 2 and
 340 A1) (Sigman et al., 1999a; DiFiore et al., 2006).

Deep convection over the shelves mixes lower $[\text{NO}_3^-]$
 and higher $\delta^{15}\text{N}$ and $\delta^{18}\text{O}$ surface waters down into the
 ocean interior, causing these dense shelf waters to be
 depleted in NO_3^- concentration and elevated in the $\delta^{15}\text{N}$
 and $\delta^{18}\text{O}$ of $\text{NO}_3^- + \text{NO}_2^-$ and NO_3^- -only relative to deep
 waters further north (Figs. 2 and 4). Because of the lower
 degree of NO_3^- consumption at the PAZ margin stations,
 the increase in NO_3^- -only and $\text{NO}_3^- + \text{NO}_2^-$ $\delta^{15}\text{N}$ and
 $\delta^{18}\text{O}$ toward the surface is small and close to the analytical
 precision. At the PAZ T_{\max} stations, a larger scatter is
 observed toward the surface but with similar mean properties
 as for the PAZ T_{\min} stations (Fig. 4). For these stations,
 the $\delta^{15}\text{N}$ or $\delta^{18}\text{O}$ of NO_3^- -only were not measured (DiFiore
 et al., 2009).

4. DISCUSSION

4.1. Nitrate supply to Antarctic surface waters

Below AASW lie two distinct water masses and, therefore,
 two different sources of NO_3^- to Antarctic Zone surface
 waters: Lower Circumpolar Deep Water (LCDW) and Upper
 Circumpolar Deep Water (UCDW), which supply NO_3^- to the
 PAZ and OAZ, respectively. UCDW is characterized on average
 by higher NO_3^- concentration and $\delta^{15}\text{N}$ than LCDW (by
 $1.5 \mu\text{mol l}^{-1}$ and 0.2–0.3‰, respectively; Sigman et al., 2000;
 DiFiore et al., 2010) but is similar in NO_3^- $\delta^{18}\text{O}$ (Figs. 2,
 4, and A1).

The NO_3^- concentration maximum in UCDW results from
 exchange with the Indian and Pacific Oceans, where
 regenerated nutrients accumulate along the mid-depth
 return flow of the ocean's “conveyor belt” circulation
 (Sarmiento et al., 2007; Talley, 2013). The ^{15}N enrichment
 in UCDW ultimately derives from the transfer (via Ekman

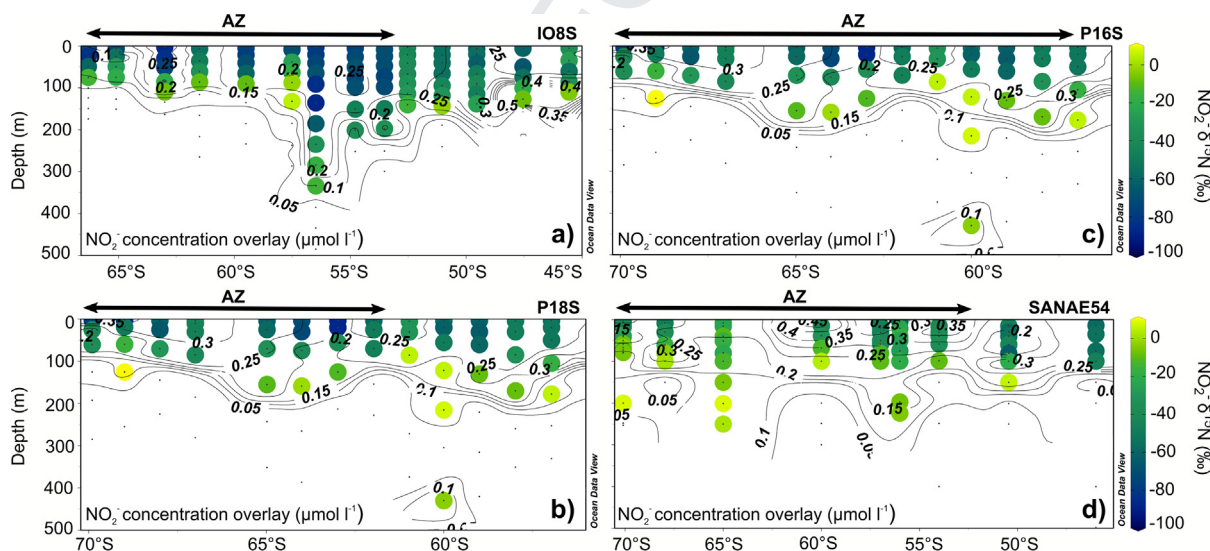


Fig. 3. Meridional depth sections of NO_2^- $\delta^{15}\text{N}$ (colored dots) with NO_2^- concentration overlay (black contours) for IO8S eastern Indian section (a), P18S eastern Pacific section (b), P16S western Pacific section (c) and SANA54 Atlantic section (d). NO_2^- $\delta^{15}\text{N}$ is shown when the NO_2^- contribution to the $\text{NO}_3^- + \text{NO}_2^-$ pool is larger than 0.25%. The black horizontal arrows above each panel indicate the Antarctic Zone. The sections were generated with Ocean Data View [Available at <http://odv.awi.de>].

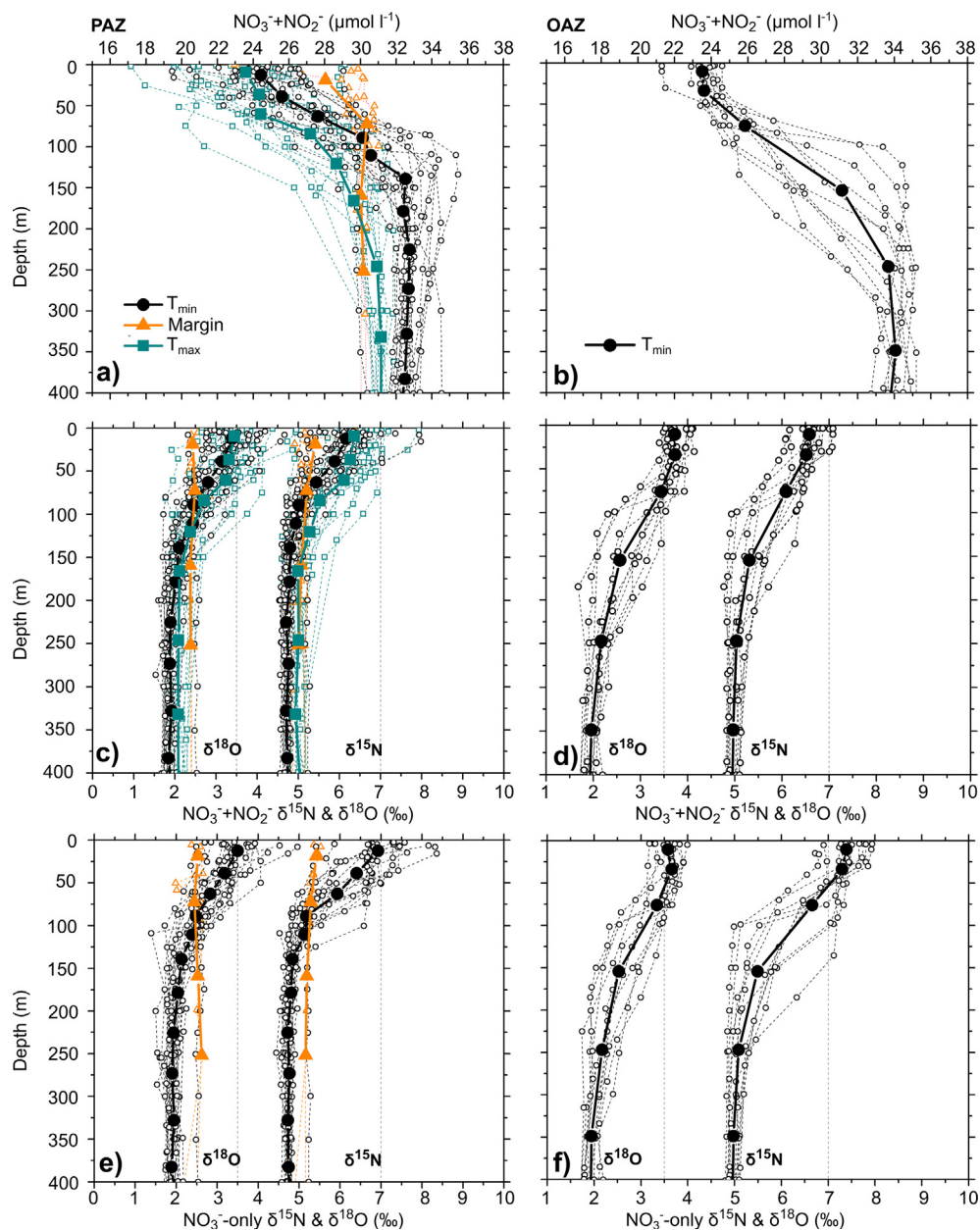


Fig. 4. Profiles of (a,b) $\text{NO}_3^- + \text{NO}_2^-$ concentration, (c,d) $\text{NO}_3^- + \text{NO}_2^-$ $\delta^{15}\text{N}$ and $\delta^{18}\text{O}$, and (e,f) NO_3^- -only $\delta^{15}\text{N}$ and $\delta^{18}\text{O}$ for the Polar Antarctic Zone (PAZ) (a,c,e) and Open Antarctic Zone (OAZ) (b,d,f) for all stations. In the PAZ, the stations are grouped by their upper ocean thermohaline structure into three categories: ' T_{\min} ' stations (white circles), 'margin' stations (orange triangles) or ' T_{\max} ' stations (green-blue squares). The mean profiles for each category are given by the corresponding solid symbols (averages for 0–20, 20–40, 40–60, 60–80, 80–100, 100–125, 125–150, 150–200, 200–300, 300–400, and 400–500 m depth intervals). All stations in the OAZ fall into the T_{\min} category.

372 transport) of ^{15}N - and ^{18}O -enriched residual NO_3^- from the
 373 polar ocean to lower latitude intermediate, thermocline,
 374 and surface waters (Fig. 2; Sigman et al., 1999a; Rafters
 375 et al., 2013). In low-latitude areas where NO_3^- consumption
 376 is complete, export production and remineralization pro-
 377 duce regenerated NO_3^- with the same $\delta^{15}\text{N}$ as the NO_3^- origi-
 378 nally supplied to the euphotic zone from the underlying
 379 thermocline. The NO_3^- in the thermocline was, in turn, ele-
 380 vated in $\delta^{15}\text{N}$ (and $\delta^{18}\text{O}$) by partial NO_3^- consumption

when the thermocline water was previously at the surface
 of the Antarctic zone (AZ), polar front zone (PFZ) and
 subantarctic zone (SAZ). Its regeneration thus elevates
 the $\delta^{15}\text{N}$ of UCDW and its deep Pacific and Indian precur-
 sors (e.g., Pacific Deep Water). The same processes do not
 elevate the NO_3^- $\delta^{18}\text{O}$ of UCDW because regenerated NO_3^-
 has a $\delta^{18}\text{O}$ equal to that of ambient water plus $\sim 1.1\text{‰}$
 (Sigman et al., 2009a; Buchwald et al., 2012), which is lower
 than the ambient NO_3^- $\delta^{18}\text{O}$ ($> 1.8\text{‰}$). Water column deni-

381
 382
 383
 384
 385
 386
 387
 388
 389

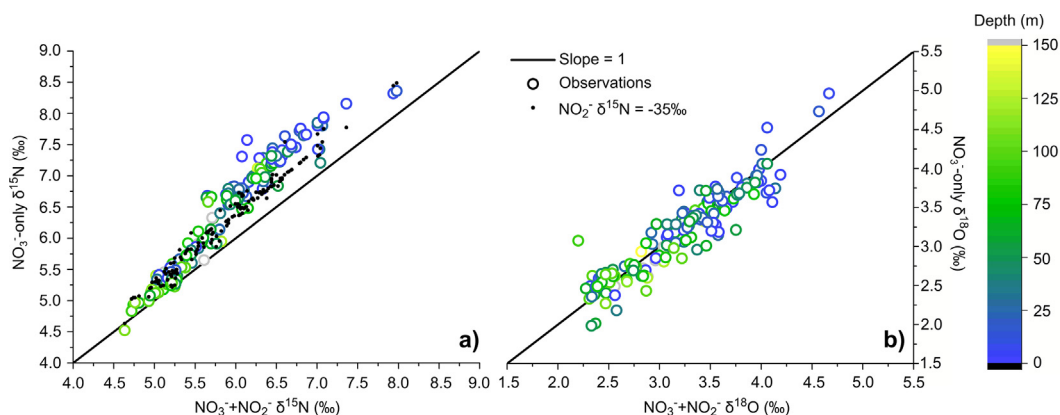


Fig. 5. Relationship between $\text{NO}_3 + \text{NO}_2$ and NO_3 -only $\delta^{15}\text{N}$ (a) and $\delta^{18}\text{O}$ (b). In (a), the black dots show the expected NO_3 $\delta^{15}\text{N}$ if NO_2 $\delta^{15}\text{N}$ was -35‰ . This NO_2 $\delta^{15}\text{N}$ value represents the minimum value expected from nitrification, NO_2 assimilation, or an imbalance in assimilatory NO_3 reduction (Fripiat et al., 2015a).

390 trification in the tropical oxygen deficient zones also works
391 to increase the NO_3^- $\delta^{15}\text{N}$ in this mid-depth return flow,
392 again causing a much weaker increase in NO_3^- $\delta^{18}\text{O}$
393 due to the low latitude NO_3^- assimilation/regeneration cycle
394 described above (Sigman et al., 2009b).

395 4.2. Nitrate isotope variation in Antarctic surface waters

396 4.2.1. Nitrite interference and the interconversion of nitrate 397 and nitrite

398 During the analysis of the NO_3^- isotopes by N_2O -based
399 methods, both NO_3^- and NO_2^- are converted to N_2O , but
400 the contribution from NO_2^- to the measured isotopic composition
401 is often considered negligible due to its typically
402 low concentration relative to NO_3^- in seawater (Sigman
403 et al., 2001; Casciotti et al., 2002; McIlvin and Altabet,
404 2005). However, in the Southern Ocean mixed layer, there
405 is commonly a small but significant accumulation of NO_2^-
406 near the surface. Most of the previous NO_3^- isotope measurements
407 in the Southern Ocean have been performed on
408 acidified samples (Sigman et al., 1999a; Altabet and
409 Francois, 2001; Karsh et al., 2003; DiFiore et al., 2006),
410 which would have affected the preservation of NO_2^- . Under
411 acidic conditions, nitrous acid (HNO_2) forms, some of
412 which may be lost to the gas phase. In addition, HNO_2
413 can decompose to nitrogen oxides (NO and NO_2), with
414 some of the NO_2 being hydrolyzed to form NO_3^- and the
415 rest escaping from the high-density polyethylene sample
416 bottles typically used for storage (Park and Lee, 1988;
417 Rayson et al., 2012). NO_2^- disappearance during storage
418 could plausibly be argued to be beneficial for the understanding
419 of the isotope dynamics associated with NO_3^-
420 assimilation, with the caveat that a portion of the HNO_2
421 breakdown can yield NO_3^- . Freezing of seawater samples
422 is thought to better preserve both NO_3^- and NO_2^- concentrations
423 as well as their $\delta^{15}\text{N}$ and $\delta^{18}\text{O}$ values, a view that
424 is supported by the stability of $\delta^{15}\text{N}$ and $\delta^{18}\text{O}$ of $\text{NO}_3^- +$
425 NO_2^- measurements in frozen samples over time (e.g.,
426 Smart et al., 2015; Kemeny et al., 2016; this study).

427 Because of the small NO_2^- contribution to the $\text{NO}_3^- +$
428 NO_2^- pool (<1%) in the Southern Ocean, prior studies

429 assumed NO_2^- to have a negligible effect on $\text{NO}_3^- + \text{NO}_2^-$
430 $\delta^{15}\text{N}$ and $\delta^{18}\text{O}$ (DiFiore et al., 2009). However, applying
431 NO_2^- removal to Southern Ocean surface mixed layer samples
432 has shown that NO_2^- can have a significant effect on
433 $\text{NO}_3^- + \text{NO}_2^-$ $\delta^{15}\text{N}$, challenging those previous assumptions
434 (Rafter et al., 2013; Smart et al., 2015; Kemeny et al., 2016).
435 This is further confirmed by our compilation, in which
436 NO_3^- -only $\delta^{15}\text{N}$ is higher than $\text{NO}_3^- + \text{NO}_2^-$ $\delta^{15}\text{N}$ by
437 $\sim 0.7 \pm 0.2\text{‰}$ in the summer surface mixed layer but is
438 not significantly different deeper in the water column
439 (Fig. 5a). Given the small contribution of NO_2^- to the NO_3^-
440 $+ \text{NO}_2^-$ pool (median = 0.9%), the $\delta^{15}\text{N}$ difference implies
441 that NO_2^- $\delta^{15}\text{N}$ is extremely low, ranging from -90‰ to
442 -17‰ (averaging $-61 \pm 20\text{‰}$) in the mixed layer and
443 increasing with depth toward $\sim 0\text{‰}$ at the T_{min} (Fig. 3).

444 NO_2^- is thought to be generated in the subsurface largely
445 as a result of the low-light conditions. Here, NO_2^- is produced
446 during the first step of nitrification ($\text{NH}_4^+ \rightarrow \text{NO}_2^-$)
447 and as a result of efflux of NO_2^- out of phytoplankton cells
448 due to an imbalance between NO_3^- and NO_2^- reduction during
449 assimilatory NO_3^- uptake. NO_2^- is consumed by both
450 the second step of nitrification ($\text{NO}_2^- \rightarrow \text{NO}_3^-$) and NO_2^-
451 assimilation by phytoplankton (Ward, 1985; Lomas and
452 Lipschultz, 2006). This combination of processes can yield
453 NO_2^- with a $\delta^{15}\text{N}$ between $\sim 0\text{‰}$ and -35‰ , depending
454 on the isotope effects of each process and their relative
455 contributions to NH_4^+ and NO_2^- removal (Fripiat et al., 2015a).
456 We observe NO_2^- $\delta^{15}\text{N}$ values that fall roughly within this
457 range in the subsurface (i.e., below the mixed layer), consistent
458 with NO_2^- being produced and consumed by the processes
459 outlined above.

460 However, another mechanism is required to produce the
461 extremely low NO_2^- $\delta^{15}\text{N}$ estimated for the surface mixed
462 layer (Fig. 3) and thus explain the measured $\delta^{15}\text{N}$ difference
463 between $\text{NO}_3^- + \text{NO}_2^-$ and NO_3^- only (Fig. 5a). Kemeny
464 et al. (2016; P16S, Fig. 1) suggested that NO_3^- - NO_2^- inter-
465 conversion can occur in the Southern Ocean mixed layer.
466 This interconversion would lead to the expression of the
467 large equilibrium N isotope effect between NO_3^- and NO_2^-
468 (60 – 90‰ under relevant conditions) (Casciotti, 2009;
469 Kemeny et al., 2016), enriching NO_3^- and depleting NO_2^-

in ^{15}N and yielding NO_3^- and NO_2^- with $\delta^{15}\text{N}$ values in the ranges that we observe (Figs. 3 and 5a). At this time, the expression of the equilibrium isotope effect between NO_3^- and NO_2^- is the only viable proposal for generating the observed extreme depletions of NO_2^- $\delta^{15}\text{N}$.

Most of the stations in both the PAZ and OAZ are found to have low NO_2^- $\delta^{15}\text{N}$ in the mixed layer, suggesting that NO_3^- – NO_2^- interconversion is ubiquitous in summer in these regions, and not only in fall as suggested by Kemeny et al. (2016). Deep mixed layers prevail in the Southern Ocean (down to ~ 100 m in December), and mixed layer depth (MLD) commonly exhibits short-term variability of up to 40 m during the summer months (Pellichero et al., 2017; Holte et al., 2017). Subsurface microbial communities (i.e., nitrifiers) may end up trapped in the mixed layer following their entrainment into it such that they spend a significant amount of time in the euphotic layer (Fripiat et al., 2015b). Once in the mixed layer with elevated levels of light, light-inhibition is likely to decrease the activity of NO_2^- oxidizers and, therefore, the unidirectional oxidation of NO_2^- to NO_3^- (Ward, 1985; Vanzella et al., 1989). Under these conditions and according to Kemeny et al. (2016), the bifunctional nitrite oxidoreductase enzyme may catalyze both the forward and reverse reactions, enriching NO_3^- and depleting NO_2^- in ^{15}N . The effective co-occurrence of NO_2^- oxidation and NO_3^- reduction in the same intracellular (or periplasmic) space could allow for the full expression of the equilibrium isotope effect at the environmental scale. While the biological catalysis of NO_3^- – NO_2^- equilibrium has previously been demonstrated in culture studies (Sundermeyer-Klinger et al., 1984; Friedman et al., 1986; Brunner et al., 2013; Wunderlich et al., 2013), the existence and operation of specific microbial consortia and enzymatic machinery that could explain our observations remains speculative.

From the perspective of the N atoms in $\text{NO}_3^- + \text{NO}_2^-$, interconversion operates as a closed system, with N atoms exchanged between NO_3^- and NO_2^- without the $\text{NO}_3^- + \text{NO}_2^-$ pool experiencing any N loss or gain. This means that $^{15}\epsilon$ associated with the assimilation of $\text{NO}_3^- + \text{NO}_2^-$ should be unaffected by NO_3^- – NO_2^- interconversion. However, as interconversion enriches NO_3^- in ^{15}N , the NO_3^- -only $^{15}\epsilon$ will be affected, and will be larger than the $\text{NO}_3^- + \text{NO}_2^-$ $^{15}\epsilon$ (Table 1; Fig. 6a and b). Consistent with Kemeny et al. (2016), we observe that the $^{15}\epsilon$ derived from NO_3^- -only profiles is higher than the $^{15}\epsilon$ derived from profiles of $\text{NO}_3^- + \text{NO}_2^-$ (Fig. 7a). However, in contrast to the observation of Kemeny et al. (2016), our larger dataset suggests that there is no relationship between MLD and the difference in $^{15}\epsilon$ estimated from the $\text{NO}_3^- + \text{NO}_2^-$ and NO_3^- -only data ($R^2 = 0.01$; p-value = 0.63) (Fig. 7a). The $^{15}\epsilon$ difference has been suggested to reflect the extent of mixed layer NO_3^- – NO_2^- interconversion at any given location. However, we hypothesize that short-term variability in the MLD provides an efficient mechanism for entrainment of the subsurface microbial communities (i.e., nitrifiers) into the euphotic layer, largely independent of the seasonal average MLD. This is likely to lead to conditions favorable for NO_3^- – NO_2^- interconversion. Moreover, the mean ($\pm 1\text{sd}$) $^{15}\epsilon$

difference (for $\text{NO}_3^- + \text{NO}_2^-$ versus NO_3^-) is similar for stations in the OAZ ($2.9 \pm 1.3\text{‰}$) and the PAZ ($2.8 \pm 1.9\text{‰}$). In the PAZ, sea-ice melting in spring-summer seeds the mixed layer with a sea-ice microbial community, which grew in a low-light environment that is favorable to nitrification (Priscu et al., 1990; Fripiat et al., 2014), and the nitrifiers of this community may also facilitate NO_3^- – NO_2^- interconversion in the mixed layer.

From the perspective of the O atoms in $\text{NO}_3^- + \text{NO}_2^-$, nitrate-nitrite interconversion implies an open system in which both the NO_3^- -only and $\text{NO}_3^- + \text{NO}_2^-$ pools are continuously supplied with O deriving predominantly from water (Kemeny et al., 2016). This is illustrated by comparing $^{18}\epsilon$ with $^{18}\epsilon$ for either NO_3^- -only or $\text{NO}_3^- + \text{NO}_2^-$. The estimates of $^{18}\epsilon$ tend to fall below the 1:1 relationship with $^{18}\epsilon$ expected from NO_3^- assimilation alone (Fig. 8; Granger et al., 2004, 2010; Karsh et al., 2012). This can be explained by the incorporation of low- $\delta^{18}\text{O}$ O atoms from ambient H_2O into either NO_2^- or NO_3^- during NO_3^- – NO_2^- interconversion (Kemeny et al., 2016). This process would propagate the low- $\delta^{18}\text{O}$ anomaly into both the $\text{NO}_3^- + \text{NO}_2^-$ and NO_3^- -only $^{18}\epsilon$, consistent with the similar values of $^{18}\epsilon$ that we estimate from the $\text{NO}_3^- + \text{NO}_2^-$ and NO_3^- -only data (Table 1; Fig. 6c and 6d). However, the very low concentration ratios of NO_2^- to NO_3^- may mask a large range in NO_2^- $\delta^{18}\text{O}$ ($\sim 50\text{‰}$) that yield no significant difference ($\pm 0.2\text{‰}$) in $\text{NO}_3^- + \text{NO}_2^-$ and NO_3^- -only $\delta^{18}\text{O}$, precluding an assessment of the O isotope systematics of NO_3^- – NO_2^- interconversion. We expect kinetic isotope effects during the incorporation and removal of O atoms, as well as equilibrium isotope effects between both NO_3^- and NO_2^- and $\text{NO}_3^- + \text{NO}_2^-$ and water (e.g., Buchwald et al., 2012).

We conclude that, in the AZ, the N isotopic composition of $\text{NO}_3^- + \text{NO}_2^-$ is more representative than that of NO_3^- -only with regard to the true isotope effect of NO_3^- assimilation because NO_3^- -only $^{15}\epsilon$ is altered during the putative NO_3^- – NO_2^- interconversion due to ^{15}N -enrichment. The $^{18}\epsilon$ estimated from both $\text{NO}_3^- + \text{NO}_2^-$ and NO_3^- -only is also vulnerable to alteration during interconversion, with O atoms likely being exchanged with water and then redistributed between NO_3^- and NO_2^- in the process.

4.2.2. Isotope fractionation during nitrate assimilation in Antarctic Surface Waters

The negative correlation between $[\text{NO}_3^-]$ and both NO_3^- $\delta^{15}\text{N}$ and $\delta^{18}\text{O}$ reflects the link between NO_3^- consumption and the NO_3^- isotopes in the Antarctic Zone (Fig. 6), whereby preferential assimilation of ^{14}N and ^{16}O by phytoplankton leaves the residual NO_3^- pool enriched in ^{15}N and ^{18}O (Sigman et al., 1999a). There is strong seasonality associated with both the supply of NO_3^- to the mixed layer and consumption by phytoplankton. Primary production and NO_3^- assimilation are restricted to the late spring and summer when total insolation is higher and surface mixed layers are shallower. Nitrate supply to the water column above the base of the winter mixed layer occurs year-round, but nitrate supply to the sunlit surface waters is dominated by wintertime vertical mixing. A high ratio of assimilation to supply is therefore expected during the productive period,

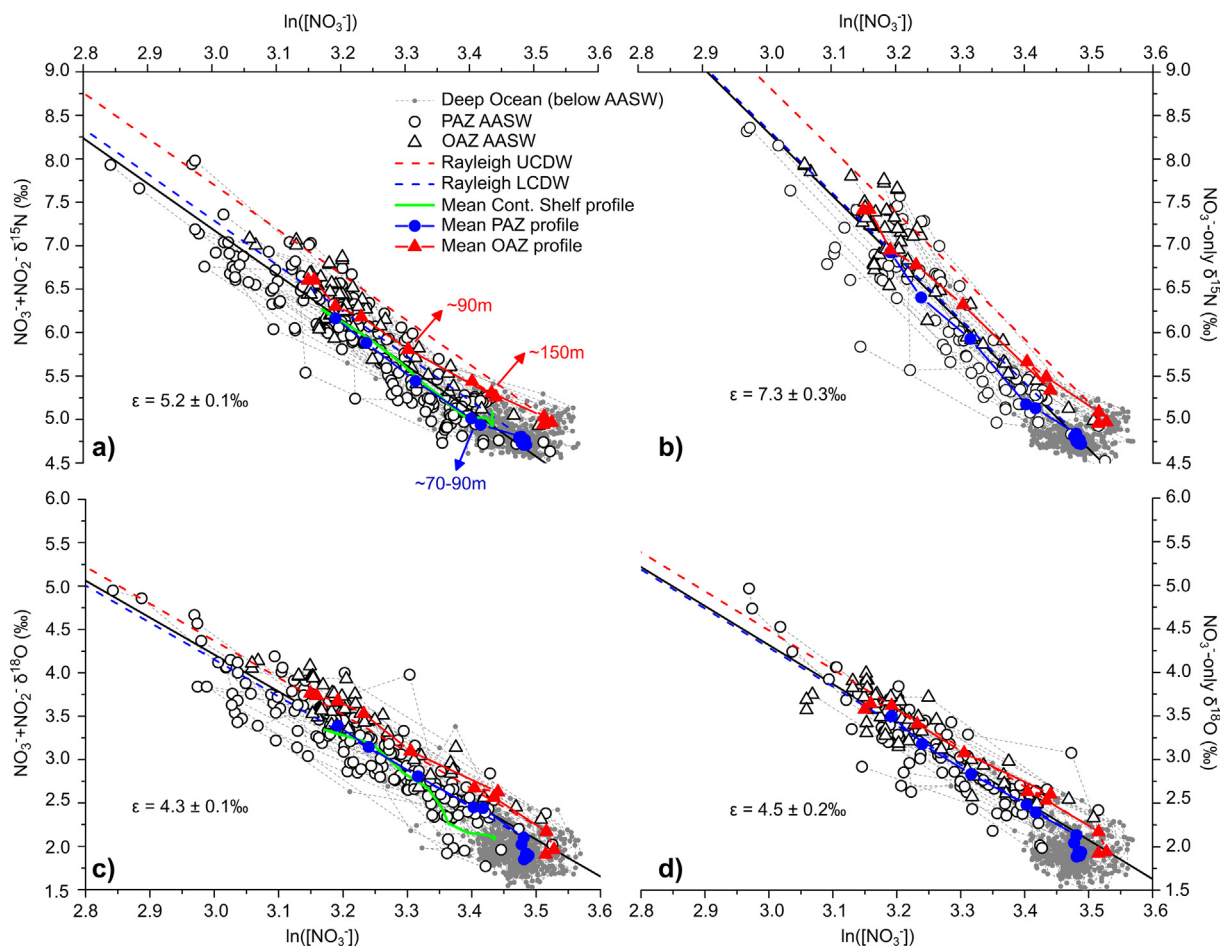


Fig. 6. Relationship between NO_3+NO_2 (a,c) and NO_3 -only (b,d) concentrations and $\delta^{15}\text{N}$ (a,b) and $\delta^{18}\text{O}$ (c,d) for AASW (empty black circles and triangles for the PAZ and OAZ, respectively) and deep water (gray circles). Red triangles and blue circles correspond to the mean OAZ and PAZ profiles (averages for 0–20, 20–40, 40–60, 60–80, 80–100, 100–125, 125–150, 150–200, 200–300, 300–400, and 400–500 m depth intervals). Regressions for AASW are indicated with the black solid lines (AASW average in Table 1), and Rayleigh fractionation trends (with LCDW and UCDW as initial conditions) with the dashed colored lines (blue and red, respectively). The mean profiles for stations near the continental shelf (i.e., ‘ T_{\max} ’ and ‘margin’ stations) are shown as green lines in (a) and (c), and are indistinguishable from the mean $\text{NO}_3 \delta^{15}\text{N}/[\text{NO}_3]$ profiles at the more pelagic ‘ T_{\min} ’ PAZ stations. In terms of $\text{NO}_3 \delta^{18}\text{O}/[\text{NO}_3]$, the stations near the continental shelf have similar surface values to the pelagic PAZ stations, but with a lower $\text{NO}_3 \delta^{18}\text{O}$ for a given NO_3 concentration deeper in the water column (i.e., below ~ 140 m).

587 and the isotope fractionation associated with nutrient consumption is likely to approximate Rayleigh fractionation
 588 kinetics (Eqs. (1)–(5), Section 2.3) (DiFiore et al., 2010;
 589 Fripiat et al., 2012). Accordingly, NO_3^- assimilation in
 590 AASW should generate a linear trend in $\text{NO}_3^- \delta^{15}\text{N}$ vs. \ln
 591 $([\text{NO}_3^-])$ and $\delta^{18}\text{O}$ vs. $\ln([\text{NO}_3^-])$ space starting from LCDW
 592 and UCDW values in the PAZ and OAZ, respectively (blue
 593 and red dashed lines in Fig. 6).

594
 595 The data generally fall on a single $\delta^{18}\text{O}/(\ln[\text{NO}_3^-])$ line
 596 consistent with a Rayleigh trend connecting deep water
 597 below AASW with the summertime mixed layer (Fig. 6c
 598 and d). In both the PAZ and OAZ, there is a similar progressive
 599 ^{18}O enrichment ($\sim 0.2\text{‰}$) in the mean profiles from
 600 the deeper layers up to below AASW, despite the lack of a
 601 clear decline in NO_3^- concentration. This small ^{18}O enrichment
 602 may be caused by the co-occurrence of partial assimilation
 603 and subsurface nitrification (Fawcett et al., 2015;

Peng et al., in press), which will cause the $\delta^{18}\text{O}$ of NO_3^-
 604 in the upper ocean to increase upwards because the assim-
 605 ilated NO_3^- is initially lower in $\delta^{18}\text{O}$ ($\sim -3\text{‰}$ to -2‰) than
 606 the regenerated NO_3^- produced by nitrification (i.e., $\sim \text{H}_2\text{O}$
 607 $\delta^{18}\text{O} + 1.1\text{‰}$; Sigman et al., 2009a,b).
 608

609 The AASW $\text{NO}_3^- \delta^{15}\text{N}/(\ln[\text{NO}_3^-])$ relationship displays
 610 upward concavity that causes T_{\min} samples to fall below a
 611 Rayleigh fractionation trend with CDW as the NO_3^- source,
 612 by 0.2‰ and 0.5‰ for the PAZ and OAZ, respectively
 613 (Fig. 6a and b) (Sigman et al., 1999a; DiFiore et al.,
 614 2010; Smart et al., 2015; Kemeny et al., 2016). Lateral
 615 exchange with waters harboring a lower $\text{NO}_3^- \delta^{15}\text{N}/(\ln$
 616 $[\text{NO}_3^-])$ relationship than CDW has been put forward to
 617 explain the OAZ T_{\min} $\delta^{15}\text{N}$ anomaly (DiFiore et al.,
 618 2010). Exchange of AASW between the PAZ and OAZ
 619 was suggested to be the most likely candidate. However, a
 620 similar albeit weaker anomaly in $\delta^{15}\text{N}$ is also observed in

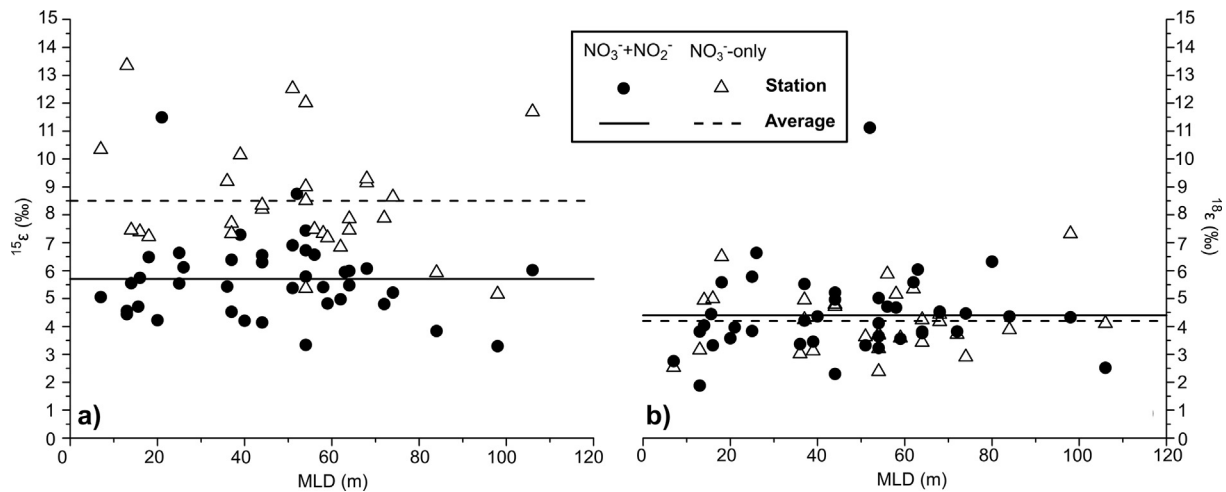


Fig. 7. $^{15}\epsilon$ (a) and $^{18}\epsilon$ (b) vs. mixed layer depth (MLD) for $\text{NO}_3^- + \text{NO}_2^-$ (black circles) and NO_3^- -only (black open circles). The solid line is for the average value of $\text{NO}_3^- + \text{NO}_2^-$ $^{15}\epsilon$ (5.7‰) and $^{18}\epsilon$ (4.4‰), and the dashed lines are for the average values of NO_3^- -only $^{15}\epsilon$ (8.4‰) and $^{18}\epsilon$ (4.2‰) (station averages in Table 1). MLD was computed based on the threshold method with a finite-density difference criterion (0.03 kg m^{-3}) from near-surface reference values (Dong et al., 2008).

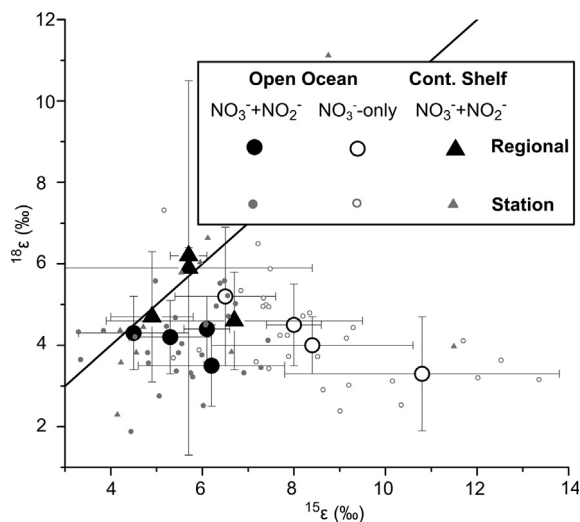


Fig. 8. $^{15}\epsilon$ vs. $^{18}\epsilon$ for $\text{NO}_3^- + \text{NO}_2^-$ (gray circles) and NO_3^- -only (gray open circles) (station averages in Table 1). NBP stations near and on the continental shelf are shown with the gray triangles (i.e., no NO_3^- -only measurements). The averages are shown with larger corresponding black symbols and error bars. The solid line is for $^{15}\epsilon = ^{18}\epsilon$.

621 the PAZ, arguing that lateral exchange cannot be the only
622 process at play. Remineralization of low- $\delta^{15}\text{N}$ PN repre-
623 sents an alternative hypothesis (Sigman et al., 1999a;
624 Smart et al., 2015). It has been suggested that regenerated
625 NO_3^- with a much lower $\delta^{15}\text{N}$ ($\sim -5 \pm 5\text{‰}$) than expected
626 from NO_3^- assimilation is required to explain the T_{min}
627 anomaly (Smart et al., 2015). Low suspended PN $\delta^{15}\text{N}$
628 has been reported for the Antarctic Zone (-4 to -2‰)
629 (Altabet and Francois, 1994a,b, 2001), with values as low
630 as -5‰ observed in late summer in the Polar Frontal Zone
631 (Lourey et al., 2003). The low PN $\delta^{15}\text{N}$ in late summer is
632 likely due to the assimilation of regenerated ^{14}N -rich

633 ammonium (Altabet, 1988; Fawcett et al., 2011) but
634 requires further investigation. When this low- $\delta^{15}\text{N}$ PN is
635 regenerated to NO_3^- upon wintertime deep mixing, it lowers
636 NO_3^- $\delta^{15}\text{N}$ throughout the (winter) mixed layer (Smart
637 et al., 2015). A related possibility is that sinking PN is rem-
638 ineralized with net isotope fractionation as it is exported
639 through the T_{min} , generating low- $\delta^{15}\text{N}$ NH_4^+ that is subse-
640 quently oxidized to NO_3^- ; this possibility will be addressed
641 in a separate manuscript.

642 Compared to the variations observed in downcore
643 diatom-bound $\delta^{15}\text{N}$ records (up to $\sim 4\text{‰}$) (Robinson and
644 Sigman, 2008; Studer et al., 2015), the NO_3^- $\delta^{15}\text{N}/(\ln$
645 $[\text{NO}_3^-])$ anomaly is small ($\sim < 0.5\text{‰}$). Nevertheless, it may
646 have repercussions for paleoceanographic reconstructions
647 (Kemeny et al., submitted for publication). Within AASW
648 from the T_{min} upward, a strong negative linear correlation
649 is observed for NO_3^- isotopes vs. $\ln([\text{NO}_3^-])$ (p-
650 value < 0.001 ; $R^2 > 0.76$), indicating that the dominant bio-
651 geochemical process at play is NO_3^- assimilation, mostly
652 occurring in the spring-summer with the shoaling of the
653 mixed layer (Sigman et al., 1999a; DiFiore et al., 2010;
654 Rafter et al., 2013). Thus, our AASW-based estimates of
655 the isotope effect (described below) are not affected by the
656 T_{min} $\delta^{15}\text{N}$ anomaly.

4.2.3. Estimating the isotope effect of nitrate assimilation in the Antarctic Zone

657 The “AASW average” isotope effects are calculated
658 using the entire AASW dataset (Table 1). “Regional aver-
659 age” isotope effects are calculated using data from individ-
660 ual cruises (IO8S, P16S, P18S, and SANAE54) or from the
661 distinct regional continental shelf settings of the NBP
662 cruises (Dumont D’Urville Sea, Davis Sea, Prydz Bay,
663 and Ross Sea). “Station average” isotope effects are esti-
664 mated by first calculating the isotope effect for each station
665 and then averaging these estimates for each cruise or regio-
666 nal setting. All estimates were calculated using Eq. (4). The
667
668

669 AASW $^{15}\epsilon$ average ($\pm 1\text{sd}$) is estimated to be $5.2 \pm 0.1\text{‰}$,
 670 with the regional $^{15}\epsilon$ averages varying from 3.2‰ to 5.9‰
 671 (Table 1). A low $^{15}\epsilon$ is reported for Dumont D'Urville
 672 Sea and Prydz Bay, both of which are characterized by
 673 small amplitudes of NO_3^- depletion ($\sim 1.7 \mu\text{mol l}^{-1}$) and
 674 ^{15}N -enrichment ($\sim 0.3\text{‰}$). These amplitudes are relatively
 675 close to the analytical precision ($\pm 2\text{sd}$) at the time when
 676 the samples from the NBP cruises were measured. Exclud-
 677 ing these two areas, the AASW $^{15}\epsilon$ average ($\pm 1\text{sd}$) is 5.4
 678 $\pm 0.2\text{‰}$, with the regional $^{15}\epsilon$ averages varying between
 679 4.8‰ and 5.9‰ . Consistent with the expected effect of
 680 NO_3^- - NO_2^- interconversion, the $^{15}\epsilon$ estimate is higher and
 681 more variable for NO_3^- -only, with an AASW $^{15}\epsilon$ average
 682 of $7.3 \pm 0.3\text{‰}$, which varies regionally from 6.2‰ to
 683 8.4‰ , similar to what has been reported previously for
 684 acidified samples from the OAZ and SAZ (Altabet and
 685 Francois, 2001; Karsh et al., 2003; DiFiore et al., 2006).
 686 We calculate values of $^{18}\epsilon$ that are lower than $^{15}\epsilon$, counter
 687 to expectations for NO_3^- assimilation (Granger et al.,
 688 2004, 2010; Rohde et al., 2015). No significant difference
 689 is observed between $\text{NO}_3^- + \text{NO}_2^-$ ($4.3 \pm 0.1\text{‰}$) and NO_3^- -
 690 only ($4.5 \pm 0.2\text{‰}$) $^{18}\epsilon$ estimates. We interpret both esti-
 691 mates to be artificially low, likely as a result of the NO_3^- -
 692 NO_2^- interconversion process.

693 Compared to the PAZ, the OAZ $\text{NO}_3^- \delta^{15}\text{N}$ vs. \ln
 694 ($[\text{NO}_3^-]$) relationship is indistinguishable in slope but is
 695 shifted upward by $\sim 0.3\text{‰}$ (Fig. 6), reflecting the $\delta^{15}\text{N}$ differ-
 696 ence in the sources of NO_3^- to the AASW in the PAZ
 697 (LCDW) and OAZ (UCDW). Despite this offset, similar
 698 isotope effects are reported for the two zones (Table 2).
 699 Over the summer months, lateral transport is likely decou-
 700 pled between the surface mixed layer and the T_{min} layer,
 701 which could bias the estimation of the isotope effect based
 702 on vertical profile data. For example, if PAZ surface waters
 703 are advected above the OAZ T_{min} , the isotope effect will be
 704 underestimated. To estimate the maximal bias associated
 705 with this decoupling, we first calculate the average NO_3^-
 706 concentration and $\delta^{15}\text{N}$ of the T_{min} and mixed layer for
 707 the PAZ and OAZ. An equal-volume mixture of PAZ
 708 and OAZ water is also considered for the T_{min} . Using this
 709 range of scenarios for T_{min} conditions (i.e., PAZ, OAZ
 710 and a mixture), we then re-estimate the isotope effects for
 711 both the OAZ and PAZ mixed layers (Table 2). The results

712 show that lateral exchange between the OAZ and PAZ can
 713 significantly bias our estimates, but that the resulting iso-
 714 tope effects are still within the range of both the full and
 715 regional datasets. Accordingly, we cannot confidently
 716 assess whether lateral transport is occurring and affecting
 717 our results.

718 A second approach is to estimate the isotope effect for
 719 each station individually. Due to the analytical precision
 720 of 0.2‰ ($\pm 2\text{sd}$), only the stations with a vertical isotopic
 721 gradient greater than 0.2‰ in the AASW are used.
 722 Regrouped by hydrographic surveys, the averages of these
 723 station-by-station estimates are not significantly different
 724 from the "regional average" isotope effects described above
 725 (Table 1). In addition, no significant relationship with
 726 MLD is observed (p-value > 0.32 ; $R^2 < 0.04$; Fig. 7), nor
 727 with sampling date (p-value > 0.34 ; $R^2 < 0.03$, data not
 728 shown).

729 By breaking the problem into a series of individual sta-
 730 tions, where each station within each region can be
 731 described with the Rayleigh model (Eq. (4)), our dataset
 732 admits one equation for each station with only two
 733 unknowns per region, which are the source NO_3^- concentra-
 734 tion and $\delta^{15}\text{N}$. We use method of least-squares to solve for
 735 these two parameters given the calculated intercept of each
 736 profile in Rayleigh space. The least-square solutions for the
 737 more pelagic stations, for which both $\text{NO}_3^- + \text{NO}_2^-$ and
 738 NO_3^- -only $\delta^{15}\text{N}$ are available (P16S, P18S, IO8S, and
 739 SANAE54), are $29.6 \pm 1.1 \mu\text{mol l}^{-1}$, $5.2 \pm 0.2\text{‰}$, and 5.6
 740 $\pm 0.3\text{‰}$ for NO_3^- concentration, $\text{NO}_3^- + \text{NO}_2^- \delta^{15}\text{N}$, and
 741 NO_3^- -only $\delta^{15}\text{N}$, respectively. These values are indistin-
 742 guishable from the mean ($\pm 1\text{sd}$) T_{min} conditions inferred
 743 from the observations at these stations: $29.6 \pm 1.9 \mu\text{mol l}^{-1}$,
 744 $5.2 \pm 0.3\text{‰}$, and $5.4 \pm 0.4\text{‰}$. This analysis further confirms
 745 that the T_{min} conditions are likely to be representative of
 746 the source conditions to the summer AZ surface waters.
 747 By including the NBP cruises, which are more representa-
 748 tive of coastal Antarctic conditions and for which only NO_3^-
 749 $+ \text{NO}_2^- \delta^{15}\text{N}$ is available, the least-square solutions are
 750 $26.8 \pm 3.8 \mu\text{mol l}^{-1}$ and $5.6 \pm 0.4\text{‰}$ for NO_3^- concentration
 751 and $\text{NO}_3^- + \text{NO}_2^- \delta^{15}\text{N}$, respectively. These values are in
 752 agreement with the lower T_{max} NO_3^- concentration (25.8
 753 $\pm 3.0 \mu\text{mol l}^{-1}$) and higher T_{max} $\text{NO}_3^- + \text{NO}_2^- \delta^{15}\text{N}$ (5.9
 754 $\pm 0.6\text{‰}$) observed at these stations.

Table 2

The effect of varying PAZ and OAZ conditions for both the T_{min} and mixed layer on the N isotope effect (Eq. (4)). In order to quantify this effect, we calculated the average NO_3^- concentration and $\delta^{15}\text{N}$ for both PAZ and OAZ T_{min} (column 1) and ML (column 2). A mixture between PAZ and OAZ (50–50%) is also considered for the T_{min} . These different conditions are inserted in Eq. (4) to calculate the N isotope effect for $\text{NO}_3^- + \text{NO}_2^-$ and NO_3^- only (column 3 and 4, respectively).

WW conditions	ML conditions	$\text{NO}_3^- + \text{NO}_2^- \ ^{15}\epsilon$ (‰)	NO_3^- -only $^{15}\epsilon$ (‰)
PAZ	PAZ	5.4	10.4
OAZ	OAZ	5.4	8.0
PAZ	OAZ	6.8	12.6
OAZ	PAZ	4.3	5.9
Mixture PAZ-OAZ	PAZ	4.8	7.8
Mixture PAZ-OAZ	OAZ	6.7	11.1
	Average	5.6	9.3
	sd	1.0	2.5

755 Averaging (\pm sd) both the regional and station $^{15}\epsilon$ averages, we estimate a nitrate assimilation isotope effect of $5.5 \pm 0.6\text{‰}$ for the Antarctic Zone, based on the $\text{NO}_3^- + \text{NO}_2^-$ measurements (Table 1). An isotope effect of $7.8 \pm 1.5\text{‰}$ is derived from the NO_3^- -only measurements; we interpret this to be artificially high due to the isotopic impacts of $\text{NO}_3^- - \text{NO}_2^-$ interconversion described above. The relative stability of the isotope effect calculated from $\text{NO}_3^- + \text{NO}_2^-$ measurements, as well as the absence of any correlation with MLD (Fig. 7a) are in disagreement with previous studies. Using a compilation of NO_3^- isotope data from the Australian sector of the Southern Ocean, DiFiore et al. (2010) observed a poleward decrease in $^{15}\epsilon$ from the SAZ to the PAZ (i.e., from $\sim 9\text{‰}$ to 5‰). However, except for the PAZ dataset, the OAZ-SAZ estimates were derived from acidified samples (Sigman et al., 1999a; Altabet and Francois, 2001; Karsh et al., 2003; DiFiore et al., 2006). DiFiore et al. (2010) hypothesized that this variation was driven by the southward shoaling of the mixed layer (Fig. 1), consistent with culture evidence for a physiological response of NO_3^- assimilation and cellular NO_3^- efflux to light availability (Needoba et al., 2004). Given our new understanding of the role of NO_2^- , we now propose that the higher OAZ $^{15}\epsilon$ estimates were due to $\text{NO}_3^- - \text{NO}_2^-$ interconversion, leading to higher apparent values of $^{15}\epsilon$ driven by the subsequent loss of NO_2^- during acidified storage in the OAZ samples (Table 1; Fig. 6a, b) (Park and Lee, 1988; Rayson et al., 2012). The spatial variability of the MLD in the Antarctic Zone is significant (Fig. 1), and MLD is likely to have been significantly different during ice ages. Thus, our finding of no impact of MLD on $^{15}\epsilon$ simplifies paleoceanographic interpretation of N isotope data in terms of the degree of NO_3^- consumption (Robinson and Sigman, 2008).

789 4.3. Comparison of nitrate-based $^{15}\epsilon$ estimates with sinking 790 PN $\delta^{15}\text{N}$ data

791 Based on the observed Rayleigh fractionation trend in
792 the AASW $\text{NO}_3^- + \text{NO}_2^-$ data and the N isotope effect of
793 NO_3^- consumption that we estimate from them (Table 1),
794 we infer an exported PN $\delta^{15}\text{N}$ of $\sim 0.4\text{‰}$ (-0.2‰ to
795 1.3‰), which is in the range of the annual-weighted sinking
796 PN $\delta^{15}\text{N}$ from sediment traps in the Antarctic Zone, -0.1‰
797 to 1.7‰ (Altabet and Francois, 2001). In contrast, if NO_3^- -
798 only data are used to estimate $^{15}\epsilon$, then the resulting export
799 production $\delta^{15}\text{N}$ is too low (-4.4‰ to -0.2‰) given the
800 constraints offered by the sediment trap data. This supports
801 our argument that the $\text{NO}_3^- + \text{NO}_2^-$ pool is more representa-
802 tive of the N available for consumption and is thus the
803 appropriate substrate pool from which to estimate $^{15}\epsilon$. This
804 is confirmed more broadly using sediment trap data from
805 both the OAZ and the Polar Frontal Zone (Altabet and
806 Francois, 2001; Lourey et al., 2003). To account for the
807 effect of varying source NO_3^- concentration and $\delta^{15}\text{N}$, the
808 difference between annual-weighted sinking PN $\delta^{15}\text{N}$ and
809 initial $\delta^{15}\text{N}$ of NO_3^- is plotted against the degree of nitrate
810 consumption ($=1-f$) (Fig. 9) (Altabet and Francois,
811 2001). Estimates of the degree of nitrate consumption are
812 based on winter to summer seasonal NO_3^- consumption,

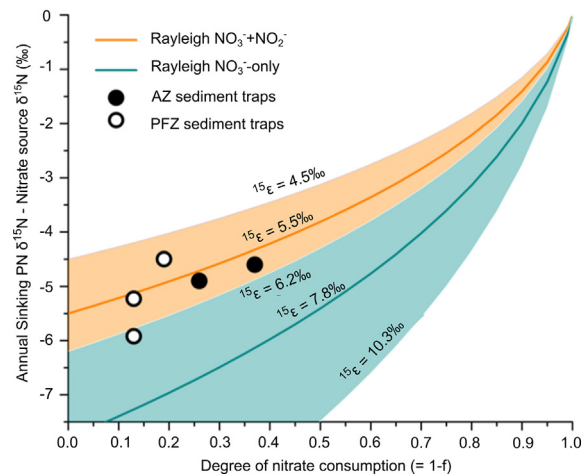


Fig. 9. Degree of nitrate consumption ($=1-f$) versus the difference between annual sinking PN and NO_3^- -source $\delta^{15}\text{N}$. Black circles show the annual-weighted sinking flux for the Antarctic Zone and white circles for the Polar Front Zone (Altabet and Francois, 2001; Lourey et al., 2003). The curved lines and shading denote AASW Rayleigh fractionation trends with varying isotope effects. The isotope effects for $\text{NO}_3^- + \text{NO}_2^-$ (mean = 5.5‰ , varying from 4.5 to 6.2‰) are shown in orange and for NO_3^- -only in blue-green (mean = 7.8‰ , varying from 6.2 to 10.3‰) (Table 1).

and initial NO_3^- $\delta^{15}\text{N}$ on winter observations in the mixed layer at the corresponding sediment trap locations. The values for both degree of nitrate consumption and initial NO_3^- $\delta^{15}\text{N}$ are given in Altabet and Francois (2001) and Lourey et al. (2003). Annual-weighted sinking PN $\delta^{15}\text{N}$ falls on the AASW Rayleigh fractionation trend for the accumulated product if the $^{15}\epsilon$ estimated from the $\text{NO}_3^- + \text{NO}_2^-$ pool is used (Fig. 9); in contrast, the trend underestimates sinking PN $\delta^{15}\text{N}$ if the $^{15}\epsilon$ estimated from the NO_3^- -only data is used. This analysis confirms a tight connection between the degree of NO_3^- consumption and the $\delta^{15}\text{N}$ of (1) $\text{NO}_3^- + \text{NO}_2^-$ and (2) export production (Sigman et al., 1999a; Altabet and Francois, 2001).

826 4.4. Paleocceanographic implications

827 The strong and consistent relationship between $\text{NO}_3^- + \text{NO}_2^-$ concentration and $\delta^{15}\text{N}$, which yields a relatively constant isotope effect in the lower range of previous estimates ($\sim 5.5 \pm 0.6\text{‰}$; from 4.5‰ to 6.2‰ , Table 1), has implications for reconstructions of the past degree of NO_3^- consumption and thus the NO_3^- concentration in Antarctic Zone surface waters (Table 3). The $\delta^{15}\text{N}$ of coral- and diatom-bound organic N in the Antarctic Zone during the last ice age was 4‰ higher than today (Sigman et al., 1999b; Robinson and Sigman, 2008; Studer et al., 2015; Wang et al., 2017), indicating elevated nitrate consumption during glacial periods (Francois et al., 1997).

839 In order to apply our new isotope effect estimates to a sedimentary diatom frustule-bound $\delta^{15}\text{N}$ record from the Pacific sector covering the last two glacial cycles (Studer et al., 2015), we need to take into account an isotopic offset between diatom-bound and sinking PN $\delta^{15}\text{N}$, recognizing

Table 3

Surface NO_3^- utilization during the last glacial maximum inferred with both $\text{NO}_3^- + \text{NO}_2^-$ and NO_3^- only $\delta^{15}\text{N}$ and $^{15}\epsilon$, as well as variations in the parameters being used to estimate this values.

	$\text{NO}_3^- + \text{NO}_2^-$	NO_3^- -only
N isotope effect ^a	4.5–6.7‰	6.2–10.8‰
Source NO_3^- $\delta^{15}\text{N}^b$	5.0–6.2‰	5.1–6.0‰
Source NO_3^- concentration ^b	24–32 $\mu\text{mol l}^{-1}$	24–32 $\mu\text{mol l}^{-1}$
Summer surface NO_3^- concentration ^c	~24 $\mu\text{mol l}^{-1}$	~24 $\mu\text{mol l}^{-1}$
Modern surface NO_3^- consumption ^d	~20%	~20%
Core-top diatom-bound $\delta^{15}\text{N}^e$	2.2‰	2.2‰
Expected sinking PN $\delta^{15}\text{N}^f$	0.4‰	-2.1‰
Isotopic offset ^g	1.8‰	4.3‰
LGM diatom-bound $\delta^{15}\text{N}^e$	6.2‰	6.2‰
LGM Expected sinking PN $\delta^{15}\text{N}^h$	4.4‰	1.9‰
LGM surface NO_3^- consumption	79–97%	53–87%
LGM summer surface NO_3^- concentration	0.7–6.7 $\mu\text{mol l}^{-1}$	3.1–15.4 $\mu\text{mol l}^{-1}$

^a Range given by the regional and station $^{15}\epsilon$ averages (Table 1).

^b Range given by the T_{min} average for each individual cruises.

^c Average for the Antarctic Zone summer mixed layer.

^d Based on the average for the Antarctic Zone T_{min} and summer mixed layer.

^e Based on Studer et al. (2015).

^f Estimated based on the AASW Rayleigh fractionation trends.

^g Difference between core-top diatom-bound and expected sinking PN $\delta^{15}\text{N}$.

^h LGM diatom-bound $\delta^{15}\text{N}$ minus the isotopic offset.

844 that bulk sinking PN is not entirely composed of diatoms
 845 and that diatom-bound N has a different isotopic composi-
 846 tion from that of bulk diatom biomass (Sigman et al.,
 847 1999b; Brunelle et al., 2007; Robinson and Sigman, 2008;
 848 Horn et al., 2011a; Morales et al., 2014). We estimate the
 849 isotopic offset from the difference (~1.8‰) between
 850 expected sinking PN $\delta^{15}\text{N}$ in the modern Antarctic Zone
 851 (~0.4‰) and core-top diatom-bound $\delta^{15}\text{N}$ (~2.2‰;
 852 Studer et al., 2015), and apply this correction to the
 853 down-core diatom-bound $\delta^{15}\text{N}$ record (Table 3). This iso-
 854 topic offset is relatively consistent, with the mean $\delta^{15}\text{N}$ off-
 855 set reported for sinking PN and core-top diatom-bound
 856 $\delta^{15}\text{N}$ in high-latitude regions (2–4‰) (Brunelle et al.,
 857 2007; Robinson and Sigman, 2008) and for net-collected
 858 bulk organic matter and diatom-bound N in the sea-ice
 859 covered water column of the Bering Shelf ($2.6 \pm 2.5\%$)
 860 (Morales et al., 2014). A similar offset (~3‰) was also
 861 recovered in a frustule cleaning study of diatoms grown
 862 for aquaculture (Morales et al., 2011), while a culture study
 863 of various species of diatoms yielded a range of offsets
 864 (Horn et al., 2011a). The higher isotope effect range sug-
 865 gested by NO_3^- -only measurements predicts lower expected
 866 sinking PN $\delta^{15}\text{N}$ (-2.1‰) and thus requires a larger iso-
 867 topic offset (4.3‰) to simulate the core-top diatom-bound
 868 $\delta^{15}\text{N}$. Changes in diatom assemblage between glacial and
 869 interglacial periods are relatively modest in the investigated
 870 record (Studer et al., 2015), implying little effect from inter-
 871 species variability on the frustule-biomass isotopic offset
 872 that may be important in other down-core records from
 873 the Atlantic sector of the Antarctic Zone (Jacot des
 874 Combes et al., 2008; Horn et al., 2011b). This is further sup-
 875 ported by assemblage-specific measurements of diatom-
 876 bound $\delta^{15}\text{N}$ through this record (Studer et al., 2015). How-
 877 ever, the controls on the frustule-biomass isotopic offset
 878 remain unclear, requiring further study.

879 Taking into account the variability encountered in the
 880 modern Antarctic Zone for the source NO_3^- $\delta^{15}\text{N}$ and iso-
 881 tope effect, we infer that the degree of NO_3^- consumption
 882 increased by ~60–80% during ice ages (Fig. 10; Table 3).
 883 The higher isotope effect range estimated from NO_3^- -only
 884 and acidified samples suggests a weaker increase (~30–
 885 65%). Our study suggests that the higher isotope effects
 886 implied by the NO_3^- -only and acidified samples are likely
 887 an artifact derived from mixed layer NO_3^- - NO_2^- intercon-
 888 version, which argues for lower ice age Antarctic surface
 889 NO_3^- concentrations (<7 $\mu\text{mol l}^{-1}$) than would have been
 890 calculated using the previous best estimates for $^{15}\epsilon$ in the
 891 Antarctic Zone (<15 $\mu\text{mol l}^{-1}$; Table 3). A separate issue
 892 is the suitability of the Rayleigh model for simulating ice
 893 age Antarctic conditions; this is addressed elsewhere
 894 (Kemeny et al., submitted for publication).

4.5. Isotope effects from different oceanic regions

895
 896 If the isotope effect estimates from NO_3^- -only data in the
 897 high-latitude regions are discarded, our estimate for the iso-
 898 topic effect of nitrate assimilation in the Antarctic Zone (5.5
 899 $\pm 0.6\%$) is similar to estimates based on the NO_3^- concen-
 900 tration/ $\delta^{15}\text{N}$ relationship in other oceanic regions (Table 4),
 901 particularly for nutrient-replete environments (4.5–6.7‰).
 902 Large variations in the MLD in high-latitude regions may
 903 provide a mechanism by which subsurface communities of
 904 nitrifying microorganisms are entrained into the mixed
 905 layer, leading to conditions favorable for NO_3^- - NO_2^- inter-
 906 conversion and thus a higher NO_3^- -only $^{15}\epsilon$ than expected
 907 from NO_3^- assimilation alone. In the Subantarctic Zone,
 908 this is supported by new measurements showing NO_2^-
 909 $\delta^{15}\text{N}$ as low as $-52 \pm 11\%$ in the mixed layer of the
 910 GOSHIP IO8S and P18S sections (data not shown). In
 911 the subarctic Pacific, this hypothesis is supported by much

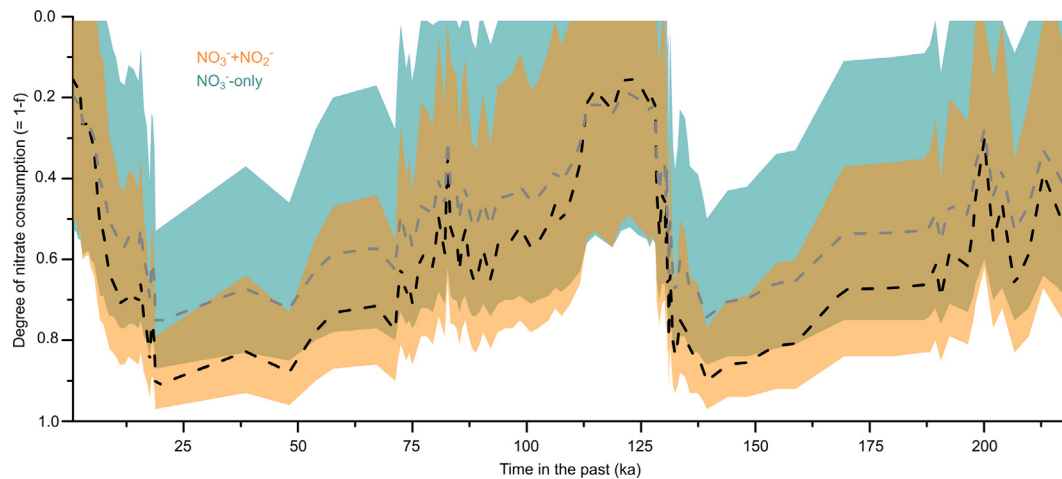


Fig. 10. Past degree of NO_3^- consumption ($= 1-f$) inferred from the AASW Rayleigh fraction trends (Fig. 6) for $\text{NO}_3^- + \text{NO}_2^-$ (orange) and NO_3^- -only (green-blue) and a diatom-bound $\delta^{15}\text{N}$ record from the Pacific sector of the Antarctic Zone, corrected for a constant isotopic offset between diatom biomass and frustule-bound N (Studer et al., 2015). The isotopic offset is taken from difference between core-top diatom-bound $\delta^{15}\text{N}$ and the expected export production $\delta^{15}\text{N}$, inferred from the AASW Rayleigh accumulated product (Table 3). The source $\text{NO}_3^- \delta^{15}\text{N}$ (T_{min}) varies from 5.0 to 6.2‰ in the case of $\text{NO}_3^- + \text{NO}_2^-$ and from 5.1 to 6.0‰ for NO_3^- -only. The ^{15}E varies from 4.5 to 6.7‰ in the case of $\text{NO}_3^- + \text{NO}_2^-$ and from 6.2 to 10.8‰ for NO_3^- -only (Table 3). The dashed black and gray lines represent the mean fractional NO_3^- depletion implied by the $\text{NO}_3^- + \text{NO}_2^-$ and NO_3^- -only isotope effects, respectively.

Table 4

Estimates of the isotope effects in different oceanic regions based on the relationship between NO_3^- concentration and $\delta^{15}\text{N}$.

	$\text{NO}_3^- + \text{NO}_2^- \text{ } ^{15}\text{E}$ (‰)	$\text{NO}_3^- \text{-only } ^{15}\text{E}$ (‰)	Study
<i>Nutrient-replete regions</i>			
Antarctic Zone	4.5–6.1	6.7–10.8	This study
Subantarctic Zone		8.0–9.0 ^a	DiFiore et al. (2006)
Subarctic Pacific	4.7–5.5		Brunelle (2009)
Subarctic Pacific		5.8–6.9	Wu et al. (1997)
Subarctic Pacific		9.1 ^a	Altabet and Francois (1994a,b)
Equatorial Pacific	5.2	3.2–6.7	Altabet (2001) and Rafter and Sigman (2016)
California Current		4.9–5.2 ^a	Altabet et al. (1999)
Subarctic North Atlantic	5.2–5.3	5.1–5.2	Peng et al. (in press)
<i>Nutrient-depleted regions</i>			
Sargasso Sea	–1.2 to 2.4	2.2–5.0	Fawcett et al. (2015)
Eastern North Atlantic	2.7	3.5	Peng et al. (in press)

^a Acidified samples only.

912 lower $\text{NO}_3^- + \text{NO}_2^- \text{ } ^{15}\text{E}$ (4.7–5.5‰) (Brunelle, 2009) than for
913 $\text{NO}_3^- \text{-only } ^{15}\text{E}$ (5.8–9.1‰) (Altabet and Francois, 1994b;
914 Wu et al., 1997).

915 In lower latitude regions, $\text{NO}_3^- \text{-only } ^{15}\text{E}$ appears to be
916 more representative than $\text{NO}_3^- + \text{NO}_2^- \text{ } ^{15}\text{E}$ of the ‘true’ iso-
917 tope effect for NO_3^- assimilation (Table 3) (Fawcett et al.,
918 2015; Rafter and Sigman, 2016), in which case the former
919 could be compared with ^{15}E estimates from acidified sam-
920 ples in similar environments (Altabet et al., 1999). The evi-
921 dence in favor of this view is that (1) $\text{NO}_3^- \text{-only}$ (rather than
922 $\text{NO}_3^- + \text{NO}_2^-$) $\delta^{15}\text{N}$ and $\delta^{18}\text{O}$ increase in unison from below
923 the euphotic zone toward the surface, in agreement with
924 NO_3^- assimilation, and (2) $\text{NO}_2^- \delta^{15}\text{N}$ is higher than in
925 AASW and thus less clearly affected by $\text{NO}_3^- \text{-NO}_2^-$ inter-
926 version (Fawcett et al., 2015; Rafter and Sigman,
927 2016; Peng et al., in press). The implication is that, rather

928 than being strongly influenced by $\text{NO}_3^- \text{-NO}_2^-$ intercon- 928
929 version, the $\delta^{15}\text{N}$ of NO_2^- at the lower latitude regions is dom- 929
930 inantly altered by other NO_2^- -oxidizing and -reducing 930
931 processes. In nutrient-depleted regions, the ^{15}E estimates 931
932 tend to be lower and more variable (Table 3). We cannot 932
933 rule out underestimation of the isotope effect due to arti- 933
934 facts from mixing in these settings. However, culture studies 934
935 report systematically lower isotope effects (<5‰) for hapt- 935
936 phytes, chlorophytes and cyanobacteria, which are the phy- 936
937 toplankton groups that are known to prevail in these 937
938 environments (Montoya and McCarthy, 1995; Granger 938
939 et al., 2010). Alternatively, at adequately low $[\text{NO}_3^-]$, there 939
940 may be a reduction in the ^{15}E of a given phytoplankton 940
941 strain (Granger et al., 2004).

942 The subarctic North Atlantic is characterized by little 942
943 difference in $\delta^{15}\text{N}$ and $\delta^{18}\text{O}$ between $\text{NO}_3^- + \text{NO}_2^-$ and 943

NO₃⁻-only (Peng et al., in press), yielding ¹⁵ε estimates of 5.2–5.3‰ and 5.1–5.2‰, respectively. In this environment, NO₂⁻ dynamics thus appear to be relatively unimportant in the isotope dynamics. [NO₂⁻] is not at appreciably lower concentration through the upper water column than in the Antarctic (Peng et al., in press). Thus, in the subarctic North Atlantic, NO₂⁻ δ¹⁵N must be far less distinct from NO₃⁻. One possible explanation is that mixed layer depth is less variable subsequent to spring/summer mixed layer shoaling, leading to less entrainment of nitrifiers into the euphotic zone and thus an overall lack of the isotopic processing that applies in the summertime Antarctic.

The overall stability of the isotope effect in nutrient-replete regions (4.5–6.7‰) contrasts with the large range of values reported from culture studies (~1–20‰) and the expected variations induced by changing NO₃⁻ metabolisms (Montoya and McCarthy, 1995; Granger et al., 2004, 2010; Needoba et al., 2004; Karsh et al., 2012, 2014). NO₃⁻ assimilation has been conceptualized as a stepwise process, in which NO₃⁻ is actively taken up through the membrane into the cell (i.e., NO₃⁻ uptake, ¹⁵ε_{upt} ~ 2‰; Karsh et al., 2014). Once inside the cell, NO₃⁻ can either be reduced by the nitrate reductase enzyme, which is thought to be the dominant fractionating step (¹⁵ε_{NR} ~ 26.6‰) or released back into the surrounding water with the isotope effect of NO₃⁻ efflux (¹⁵ε_{eff} ~ 1.2‰) (Karsh et al., 2012, 2014). Any imbalance between NO₃⁻ uptake and intracellular reduction allows ¹⁵N-enriched NO₃⁻, which is accumulated inside the cell (e.g., in the vacuole), to be released via NO₃⁻ efflux, transmitting the ¹⁵N-enrichment to seawater NO₃⁻ (Needoba et al., 2004). Given the enzyme-level isotope effects available in the literature, the organism-level isotope effect lies between ~2‰ (¹⁵ε_{upt}) and ~25.8‰ (¹⁵ε_{upt} + ¹⁵ε_{NR} - ¹⁵ε_{eff}) for an efflux/uptake ratio of 0 and 1, respectively (Karsh et al., 2012, 2014). An isotope effect between 4.5‰ and 6.7‰ argues for a small and relatively constant (0.10–0.27) efflux/uptake ratio in nutrient-replete regions (Table 3), with the caveat that the isotope effect provides an integrative measure of seasonal NO₃⁻ consumption and therefore a succession of different phytoplankton assemblages and NO₃⁻ metabolisms. Lower isotope effects in nutrient-depleted regions may point to an efflux/uptake ratio less than 0.05, with most of the isotope fractionation driven by NO₃⁻ uptake. However, as described above, we cannot rule out underestimation of the isotope effect due to artifacts resulting from mixing in these low-nutrient settings.

5. CONCLUSIONS AND REMAINING QUESTIONS

We report a relatively constant isotope effect for summertime NO₃⁻ assimilation in the modern Antarctic Zone (5.5 ± 0.6‰), representative of the full seasonal NO₃⁻ depletion and the associated range of physical properties encountered in this region of the Southern Ocean. This implies a tight connection between the degree of NO₃⁻ consumption and the δ¹⁵N of both the NO₃⁻ pool and the export flux. These findings contradict previous studies that reported variability in the isotope effect due to varying environmental conditions (i.e. mixed layer depth), and simplify the

effort to reconstruct the degree of NO₃⁻ consumption in the Antarctic Zone at times in the past.

We suggest that the variability reported in previous studies is due to a methodological artifact, induced by putative NO₃⁻–NO₂⁻ interconversion in the mixed layer. Although the systematics of NO₃⁻–NO₂⁻ interconversion are relatively straightforward for the N isotopes, operating as a closed system where N atoms are exchanged between NO₃⁻ and NO₂⁻ and expressing a large equilibrium N isotope effect, the systematics applicable to the O isotopes remain unknown. No clear difference is reported between NO₃⁻–NO₂⁻ and NO₃⁻-only δ¹⁸O. However, the small contribution (0.7 ± 0.2‰) of NO₂⁻ to the NO₃⁻ + NO₂⁻ pool may mask large differences in NO₂⁻ δ¹⁸O (~50‰) that yield no significant differences (±0.2‰) in NO₃⁻ + NO₂⁻ and NO₃⁻-only δ¹⁸O. Kinetic isotope effects during the incorporation and removal of O atoms are expected, as well as equilibrium isotope effects between NO₃⁻ and NO₂⁻ as well as between NO₃⁻–NO₂⁻ and water. However, the full elucidation of these systematics requires the measurement of the δ¹⁸O of NO₂⁻ immediately upon sample collections (e.g., Buchwald et al., 2015).

Another open question for future studies concerns the higher N isotope effect estimates previously reported for the Subantarctic Zone, also based on measurements from acidified samples (DiFiore et al., 2006, 2010). It remains possible that the particularly deep mixed layers of the SAZ are adequate for light limitation to cause a higher ¹⁵ε for nitrate assimilation, as observed in culture experiments (Needoba et al., 2004). However, new measurements of both NO₃⁻ + NO₂⁻ and NO₃⁻-only δ¹⁵N on the GOSHIP IO8S and P18S sections indicate that NO₃⁻–NO₂⁻ interconversion also occurs in the SAZ mixed layer, with NO₂⁻ δ¹⁵N estimated to be as low as -52 ± 11‰ (data not shown). Thus, artifacts related to NO₂⁻ loss during storage have likely also raised the measured NO₃⁻ δ¹⁵N and thus the estimates of ¹⁵ε in this zone of the Southern Ocean as well. A model taking into account the NO₃⁻ supplies from both the south and the underlying SAZ thermocline is required to tackle this question.

UNCITED REFERENCES

Marshall and Speer (2012), Möbius (2013), and Rohde et al. (2008).

ACKNOWLEDGMENTS

The new stable isotope data for the GOSHIP section IO8S and P18S presented in this study will be merged into the IO8S and P18S CCHDO product (<https://cchdo.ucsd.edu/>). We thank the ship captains, crews, and chief scientists (R.V. Roger Revelle, R.V. Ronald H. Brown, and R.V. SA Agulhas II) who supported the sampling activities during the various field programs that contributed to this study. We are also grateful to M.A. Weigand (Princeton University) for methodological advice and Barbara Hinnenberg (MPIC) for help with sample processing. This study was funded by the Max Planck Society. SEF thanks the South African National Research Foundation and Antarctic Programme (through grants 105539 and 110735). DMS acknowledges US NSF grant 1401489, as well as 0960802, 0992345, 0612198. P.C.

1059 K. acknowledges support from the Fannie & John Hertz Founda-
1060 tion and the Department of Defense NDSEG Fellowship.
1061

1062 APPENDIX A. SUPPLEMENTARY MATERIAL

1063 Supplementary data to this article can be found online at
1064 <https://doi.org/10.1016/j.gca.2018.12.003>.

1065 REFERENCES

1066 Abernathey R. and Ferreira D. (2015) Southern Ocean isopycnal
1067 mixing and ventilation changes driven by winds. *Geophys. Res.*
1068 *Lett.* **43**, 10357–10365. <https://doi.org/10.1002/2015GL066238>.
1069 Altabet M. A. (1988) Variations in nitrogen isotopic composition
1070 between sinking and suspended particles: implications for
1071 nitrogen cycling and particle transformation in the open ocean.
1072 *Deep-Sea Res.* **35**(4), 535–554.
1073 Altabet M. A. and Francois R. (1994a) Sedimentary nitrogen
1074 isotopic ratio as a recorder for surface ocean nitrate utilization.
1075 *Global Biogeochem. Cy.* **8**(1), 103–116.
1076 Altabet M. A. and Francois R. (1994b) The use of nitrogen isotopic
1077 ratio for reconstruction of past change in surface ocean nutrient
1078 utilization. In *Carbon Cycling in the Glacial Ocean: Constraints*
1079 *on the Ocean's Role in Global Change* (eds. R. Zahn, M.
1080 Kaminski, L. Labeyrie and T. F. Pederson). Springer-Verlag,
1081 pp. 281–306.
1082 Altabet M. A., Pilskaal C., Thunell R., Pride C., Sigman D. M.,
1083 Chavez F. and Francois R. (1999) The nitrogen isotope
1084 biogeochemistry of sinking particles from the margin of the
1085 Eastern North Pacific. *Deep Sea Res. I* **46**, 655–679.
1086 Altabet M. A. and Francois R. (2001) Nitrogen isotope biogeo-
1087 chemistry of the Antarctic Polar Frontal Zone at 170°W. *Deep-*
1088 *Sea Res. II* **48**, 4247–4273.
1089 Altabet M. A. (2001) Nitrogen isotopic evidence for micronutrient
1090 control of fractional NO₃ utilization in the equatorial Pacific.
1091 *Limnol. Oceanogr.* **46**(2), 368–380.
1092 Böhlke J. K., Mroczkowski S. J. and Coplen T. B. (2003) Oxygen
1093 isotopes in nitrate: new reference materials for ¹⁸O:¹⁷O:¹⁶O
1094 measurements and observations on nitrate-water equilibration.
1095 *Rapid Commun. Mass Spectrom.* **17**, 1835–1846.
1096 Brunelle B. G., Sigman D. M., Cook M. S., Keigwin L. D., Haug
1097 G. H., Plessen B., Schettler G. and Jaccard S. L. (2007)
1098 Evidence from diatom-bound nitrogen isotopes for subarctic
1099 Pacific stratification during the last ice age and a link to North
1100 Pacific denitrification changes. *Paleoceanography* **22**, PA1215.
1101 <https://doi.org/10.1029/2005PA001205>.
1102 Brunelle B. G. (2009) *Nitrogen isotope constraints on the biogeo-*
1103 *chemistry and paleoclimatology of the Subarctic North Pacific*
1104 Ph.D. Thesis. Princeton Univ..
1105 Brunner B., Contreras S., Lehmann M. F., Matantseva O., Røllög
1106 M., Kalvelage T., Klockgether G., Lavik G., Jetten M. S. M.,
1107 Kartal B. and Kuypers M. M. M. (2013) Nitrogen isotope
1108 effects induced by anammox bacteria. *PNAS* **110**(47), 18994–
1109 18999.
1110 Buchwald C., Santoro A. E., McIlvin M. R. and Casciotti K. L.
1111 (2012) Oxygen isotopic composition of nitrate and nitrite
1112 produced by nitrifying cocultures and natural marine assem-
1113 blages. *Limnol. Oceanogr.* **57**(5), 1361–1375.
1114 Buchwald C., Santoro A. E., Stanley R. H. R. and Casciotti K. L.
1115 (2015) Nitrogen cycling in the secondary nitrite maximum of
1116 the eastern tropical North Pacific off Costa Rica. *Global*
1117 *Biogeochem. Cycles* **29**, 2061–2081. [https://doi.org/10.1002/](https://doi.org/10.1002/2015GB005187)
1118 [2015GB005187](https://doi.org/10.1002/2015GB005187).

Casciotti K. L., Sigman D. M., Galanter M., Hasting M., Böhlke J. 1119
K. and Hilkert A. (2002) Measurement of the oxygen isotopic 1120
composition of nitrate in seawater and freshwater using the 1121
denitrifier method. *Anal. Chem.* **74**, 4905–4912. 1122
Casciotti K. L., Trull T. W., Glover D. M. and Davies D. (2008) 1123
Constraints on nitrogen cycling at the subtropical North Pacific 1124
Station ALOHA from isotopic measurements of nitrate and 1125
particulate nitrogen. *Deep-Sea Res. II* **55**, 1661–1672. 1126
Casciotti K. L. (2009) Inverse kinetic isotope fractionation during 1127
bacterial nitrite oxidation. *Geochim. Cosmochim. Acta* **73**(7), 1128
2061–2076. <https://doi.org/10.1016/j.gca.2008.12.022>. 1129
DiFiore P. J., Sigman D. M., Trull T. W., Lourey M. J., Karsh K., 1130
Cane G. and Ho R. (2006) Nitrogen isotope constraints on 1131
subantarctic biogeochemistry. *J. Geophys. Res.* **111**, C08016. 1132
<https://doi.org/10.1029/2005JC003216>. 1133
DiFiore P. J., Sigman D. M. and Dunbar R. B. (2009) Upper ocean 1134
nitrogen fluxes in the Polar Antarctic Zone: constraints from 1135
the oxygen and nitrogen isotopes of nitrate. *Geochem. Geophys.* 1136
Geosyst. **10**, Q11016. <https://doi.org/10.1029/2009GC002468>. 1137
DiFiore P. J., Sigman D. M., Karsh K. L., Trull T. W., Dunbar R. 1138
B. and Robinson R. S. (2010) Poleward decrease in the isotope 1139
effect of nitrate assimilation across the Southern Ocean. 1140
Geophys. Res. Lett. **37**, L17601. [https://doi.org/10.1029/](https://doi.org/10.1029/2010GL044090)
1141 [2010GL044090](https://doi.org/10.1029/2010GL044090). 1142
Dong S., Sprintall J., Gille S. T. and Talley L. (2008) Southern 1143
Ocean mixed-layer depth from Argo float profiles. *J. Geophys.* 1144
Res. **113**, C06013. <https://doi.org/10.1029/2006JC004051>. 1145
Fawcett S. E., Lomas M. W., Casey J. R., Ward B. B. and Sigman 1146
D. M. (2011) Assimilation of upwelled nitrate by small 1147
eukaryotes in the Sargasso Sea. *Nat. Geosci.* **4**. [https://doi.](https://doi.org/10.1038/NNGEO01265)
1148 [org/10.1038/NNGEO01265](https://doi.org/10.1038/NNGEO01265). 1149
Fawcett S. E., Ward B. B., Lomas M. W. and Sigman D. M. (2015) 1150
Vertical decoupling of nitrate assimilation and nitrification in 1151
the Sargasso Sea. *Deep-Sea Res. I* **103**, 64–72. 1152
Francois R., Altabet M. A., Yu E.-F., Sigman D. M., Bacon M. P., 1153
Frank M., Bohrmann G., Bareille G. and Labeyrie L. D. (1997) 1154
Contribution of Southern Ocean surface-water stratification to 1155
low atmospheric CO₂ concentration during the last glacial 1156
period. *Nature* **389**, 929–935. 1157
Friedman S. H., Massefki, Jr., W. and Hollocher T. C. (1986) 1158
Catalysis of intermolecular oxygen atom transfer by nitrite 1159
dehydrogenase of *Nitrobacter agilis*. *J. Biol. Chem.* **261**(23), 1160
10538–10543. 1161
Fripiat F., Cavagna A.-J., Dehairs F., de Brauwere A., André L. 1162
and Cardinal D. (2012) Processes controlling the Si-isotopic 1163
composition in the Southern Ocean and application for 1164
paleoceanography. *Biogeosciences* **9**, 2443–2457. 1165
Fripiat F., Sigman D. M., Fawcett S. E., Rafter P. A., Weigand M. 1166
A. and Tison J.-L. (2014) New insights into sea ice nitrogen 1167
biogeochemical dynamics from the nitrogen isotopes. *Global* 1168
Biogeochem. Cy. **28**. <https://doi.org/10.1002/2013GB004729>. 1169
Fripiat F., Sigman D. M., Massé G. and Tison J.-L. (2015a) High 1170
turnover rates indicated by changes in the fixed N forms and 1171
their stable isotopes in Antarctic landfast sea ice. *J. Geophys.* 1172
Res. Oceans **120**. <https://doi.org/10.1002/2014JC010583>. 1173
Fripiat F., Elskens M., Trull T. W. and Blain S., et al. (2015b) 1174
Significant mixed layer nitrification in a natural iron-fertilized 1175
bloom of the Southern Ocean. *Global Biogeochem. Cy.* **29**. 1176
<https://doi.org/10.1002/2014GB005051>. 1177
Granger J., Sigman D. M., Needoba J. A. and Harrison P. J. (2004) 1178
Coupled nitrogen and oxygen isotope fractionation of nitrate 1179
during assimilation by cultures of marine phytoplankton. 1180
Limnol. Oceanogr. **49**(5), 1763–1773. 1181
Granger J. and Sigman D. M. (2009) Removal of nitrite with 1182
sulfamic acid for nitrate N and O isotope analysis with the 1183

- denitrifier method. *Rapid Commun. Mass Spectrom.* **23**, 3753–3762.
- Granger J., Sigman D. M., Rohde M. M., Maldonado M. T. and Tortell P. D. (2010) N and O isotope effects during nitrate assimilation by unicellular prokaryotic and eukaryotic plankton cultures. *Geochim. Cosmochim. Acta* **74**, 1030–1040.
- Holte J., Talley L. D., Gilson J. and Roemmich D. (2017) An Argo mixed layer climatology and database. *Geophys. Res. Lett.* **44**, 5618–5626. <https://doi.org/10.1002/2017GL073426>.
- Horn M. G., Robinson R. S., Rynearson T. A. and Sigman D. M. (2011a) Nitrogen isotopic relationship between diatom-bound and bulk organic matter of cultured polar diatoms. *Paleoceanography* **26**, PA3208. <https://doi.org/10.1029/2010PA002080>.
- Horn M. G., Robinson R. S., Rynearson T. A. and Sigman D. M. (2011b) Nitrogen isotopic relationship between diatom-bound and bulk organic matter of cultured polar diatoms. *Paleoceanography* **26**, PA3208. <https://doi.org/10.1029/2010PA002080>.
- Jaccard S. L., Hayes C. T., Martinez-Garcia A., Hodell D. A., Anderson R. F., Sigman D. M. and Haug G. H. (2013) Two modes of change in Southern Ocean productivity over the past million years. *Science* **339**, 1419–1423.
- Jacot Des Combes H., Esper O., De La Rocha C. L., Abelman A., Gersonde R., Yam R. and Shemesh A. (2008) Diatom $\delta^{13}\text{C}$, $\delta^{15}\text{N}$, and C/N since the Last Glacial Maximum in the Southern Ocean: potential impact of species composition. *Paleoceanography* **23**, PA4209. <https://doi.org/10.1029/2008PA001589>.
- Karsh K. L., Trull T. W., Lourey M. J. and Sigman D. M. (2003) Relationship of nitrogen isotope fractionation to phytoplankton size and iron availability during the Southern Ocean Iron Release Experiment (SOIREE). *Limnol. Oceanogr.* **48**(3), 1058–1068.
- Karsh K. L., Granger J., Kritee K. and Sigman D. M. (2012) Eukaryotic Assimilatory Nitrate Reducase fractionates N and O isotopes with a ratio near unity. *Environ. Sci. Technol.* **46**, 5727–5735.
- Karsh K. L., Trull T. W., Sigman D. M., Thompson P. A. and Granger J. (2014) The contributions of nitrate uptake and efflux to isotope fractionation during algal nitrate assimilation. *Geochim. Cosmochim. Acta* **132**, 391–412.
- Kemeny P. C., Weigand M. A., Zhang R., Carter B. R., Karsh K. L., Fawcett S. E. and Sigman D. M. (2016) Enzyme-level interconversion of nitrate and nitrite in the fall mixed layer of the Antarctic Ocean. *Global Biogeochem. Cy.* **30**, 1069–1085. <https://doi.org/10.1002/2015GB005350>.
- Kemeny P. C., Kast E. R., Hain M. P., Fawcett S. E., Fripiat F., Studer A. S., Martinez-Garcia A., Haug G. H. and Sigman D. M. (meny et al., submitted for publication) A seasonal model of nitrogen isotopes in the ice age Antarctic Zone: support for reduced upper cell overturning. *Paleoceanography and Paleoclimatology*. (submitted for publication).
- Kohfeld K. E., Le Quééré C., Harrison S. P. and Anderson R. F. (2005) Role of marine biology in glacial-interglacial CO_2 cycles. *Science* **308**, 74–78.
- Lomas M. W. and Lipschultz F. (2006) Forming the primary nitrite maximum: nitrifiers or phytoplankton? *Limnol. Oceanogr.* **51**, 2453–2467.
- Lourey M. J., Trull T. W. and Sigman D. M. (2003) Sensitivity of $\delta^{15}\text{N}$ of nitrate, surface suspended and deep sinking particulate nitrogen to seasonal nitrate depletion in the Southern Ocean. *Global Biogeochem. Cy.* **17**(3), 1081. <https://doi.org/10.1029/2002GB001973>.
- Mariotti A., Germon J. C., Hubert P., Kaiser P., Letolle R., Tardieux A. and Tardieux P. (1981) Experimental determination of nitrogen kinetic isotope fractionation: some principles; illustration for the denitrification and nitrification processes. *Plant Soil* **62**, 413–430.
- Marshall J. and Speer K. (2012) Closure of the meridional overturning circulation through Southern Ocean upwelling. *Nat. Geosci.* **5**. <https://doi.org/10.1038/NNGEO1391>.
- Martin J. H., Gordon R. M. and Fitzwater S. E. (1990) Iron in Antarctic waters. *Nature* **345**, 156–158.
- Martinez-Garcia A., Sigman D. M., Ren H., Anderson R. F., Straub M. S., Hodell D. A., Jaccard S. L., Eglinton T. I. and Haug G. H. (2014) Iron fertilization of the Subantarctic Ocean during the last ice age. *Science* **343**, 1347–1350.
- McIlvin M. R. and Altabet M. A. (2005) Chemical conversion of nitrate and nitrite to nitrous oxide for nitrogen and oxygen isotopic analysis in freshwater and seawater. *Anal. Chem.* **77**, 5589–5595.
- Mitchel B. G., Brody E. A., Holm-Hansen O., McClain C. and Bishop J. (1991) Light limitation of phytoplankton and macronutrient utilization in the Southern Ocean. *Limnol. Oceanogr.* **36**, 1662–1677.
- Möbius J. (2013) Isotope fractionation during nitrogen remineralization (ammonification): Implications for nitrogen isotope biogeochemistry. *Geochim. Cosmochim. Acta* **105**, 422–432.
- Montoya J. P. and McCarthy J. J. (1995) Isotopic fractionation during nitrate uptake by phytoplankton grown in continuous culture. *J. Plankton Res.* **17**(3), 439–464.
- Morales L. V., Granger J., Chang B. X., Prokopenko M. G., Plessen B., Gradinger R. and Sigman D. M. (2014) Elevated $^{15}\text{N}/^{14}\text{N}$ in particulate organic matter, zooplankton, and diatom frustule-bound nitrogen in the ice-covered water column of the Bering Sea eastern shelf. *Deep-Sea Res. II* **109**, 100–111.
- Needoba J. A., Sigman D. M. and Harrison P. J. (2004) The mechanism of isotope fractionation during algal nitrate assimilation as illuminated by the $^{15}\text{N}/^{14}\text{N}$ of intracellular nitrate. *J. Phycol.* **40**, 517–522.
- Orsi A. H., Whitworth, III, T. and Nowlin, Jr., W. D. (1995) On the meridional extent and fronts of the Antarctic Circumpolar Current. *Deep-Sea Res. I* **42**(5), 641–673.
- Park J.-Y. and Lee Y.-N. (1988) Solubility and decomposition kinetics of nitrous acid in aqueous solution. *J. Phys. Chem.* **92**, 6294–6302.
- Pellichero V., Sallée J.-B., Schmidtko S., Roquet F. and Charrassin J.-B. (2017) The ocean mixed layer under Southern Ocean sea-ice: Seasonal cycle and forcing. *J. Geophys. Res.* **122**, 1608–1633. <https://doi.org/10.1002/2016JC011970>.
- Peng X., Fawcett S. E., van Oostende N., Wolf M. J., Marconi D., Sigman D. M. and Ward B. B. (in press) Nitrogen uptake and nitrification in the subarctic North Atlantic Ocean (in press). *Limnol. Oceanogr.* <https://doi.org/10.1002/lno.10784>.
- Priscu J. C., Downes M. T., Priscu L. R., Palmisano A. C. and Sullivan C. W. (1990) Dynamic of ammonium oxidizer activity and nitrous oxide (N_2O) within and beneath Antarctic sea ice. *Mar. Ecol. Prog. Ser.* **62**, 37–46.
- Rafter P. A., DiFiore P. J. and Sigman D. M. (2013) Coupled nitrogen and oxygen isotopes and organic matter remineralization in the Southern and Pacific Oceans. *J. Geophys. Res.* **118**, 1–14. <https://doi.org/10.1002/jgrc.20316>.
- Rafter P. A. and Sigman D. M. (2016) Spatial distribution and temporal variation of nitrate nitrogen and oxygen isotopes in the upper equatorial Pacific Ocean. *Limnol. Oceanogr.* **61**, 14–31.
- Raymond B. (2014) The maximum extent of sea ice in the southern hemisphere by day and winter season. Australian Data Center – CAASM Metadata (<http://data.aad.gov.au/aadc/metadata/>)

- 1315 [metadata_redirect.cfm?md=/AMD/AU/sea_ice_extent_](#)
1316 [winter](#)).
- 1317 Rayson M. S., Mackie J. C., Kennedy E. M. and Dlugogorski B. Z.
1318 (2012) Accurate rate constants for decomposition of aqueous
1319 nitrous acid. *Inorg. Chem.* **51**, 2178–2185.
- 1320 Robinson R. S. and Sigman D. M. (2008) Nitrogen isotopic
1321 evidence for a poleward decrease in surface nitrate within the
1322 ice age Antarctic. *Quater. Sci. Rev.* **27**, 1076–1090.
- 1323 Rohde M. M., Granger J., Sigman D. M. and Lehmann M. F.
1324 (2008) Coupled nitrate N and O stable isotope fractionation by
1325 a natural marine plankton consortium. *Front. Mar. Sci.* **2**, 28.
1326 <https://doi.org/10.3389/fmars.2015.00028>.
- 1327 Sarmiento J. L., Gruber N., Brzezinski M. A. and Dunne J. P.
1328 (2004) High-latitude controls of thermocline nutrients and low
1329 latitude biological productivity. *Nature* **427**, 56–60.
- 1330 Sarmiento J. L., Simeon J., Gnanadesikan A., Gruber N., Key R.
1331 M. and Schlitzer R. (2007) Deep ocean biogeochemistry of
1332 silicic acid and nitrate. *Global Biogeochem. Cy.* **21**, GB1S90.
1333 <https://doi.org/10.1029/2006GB002720>.
- 1334 Sigman D. M., Altabet M. A., McCorkle D. C., Francois R. and
1335 Fisher G. (1999a) The $\delta^{15}\text{N}$ of nitrate in the Southern Ocean:
1336 consumption of nitrate in surface waters. *Global Biogeochem.*
1337 *Cy.* **13**(4), 1149–1166.
- 1338 Sigman D. M., Altabet M. A., Francois R., McCorkle D. C. and
1339 Gaillard J.-F. (1999b) The isotopic composition of diatom-
1340 bound nitrogen in Southern Ocean sediments. *Paleoceanogr.* **14**
1341 (2), 118–134.
- 1342 Sigman D. M., Altabet M. A., McCorkle D. C., Francois R. and
1343 Fisher G. (2000) The $\delta^{15}\text{N}$ of nitrate in the Southern Ocean:
1344 nitrogen cycling and circulation in the ocean interior. *J.*
1345 *Geophys. Res.* **105**(C8), 19599–19614.
- 1346 Sigman D. M., Casciotti K. L., Andreani M., Barford C., Galanter
1347 M. and Böhlke J. K. (2001) A bacterial method for the nitrogen
1348 isotopic analysis of nitrate in seawater and freshwater. *Anal.*
1349 *Chem.* **73**, 4145–4153.
- 1350 Sigman D. M., DiFiore P. J., Hain M. P., Deutsch C., Wang Y.,
1351 Karl D. M., Knapp A. N., Lehmann M. F. and Pantoja S.
1352 (2009a) The dual isotopes of deep nitrate as a constraint on the
1353 cycle and budget of oceanic fixed nitrogen. *Deep-Sea Res. I* **56**,
1354 1419–1439.
- 1355 Sigman D. M., DiFiore P. J., Hain M. P., Deutsch C. and Karl D.
1356 M. (2009b) Sinking organic matter spreads the nitrogen isotope
1357 signal of pelagic denitrification in the North Pacific. *Geophys.*
1358 *Res. Lett.* **36**, L08605. <https://doi.org/10.1029/2008GL035784>.
- 1359 Sigman D. M., Hain M. P. and Haug G. H. (2010) The polar ocean
1360 and glacial cycles in atmospheric CO_2 concentration. *Nature*
1361 **466**. <https://doi.org/10.1038/nature09149>.
- 1362 Smart S. M., Fawcett S. E., Thomalla S. J., Weigand M. A.,
1363 Reason C. J. C. and Sigman D. M. (2015) Isotopic evidence for
nitrification in the Antarctic winter mixed layer. *Global*
Biogeochem. Cy. **29**. <https://doi.org/10.1002/2014GB005013>.
- Studer A. S., Sigman D. M., Martinez-Garcia A., Benz V.,
Winckler G., Kuhn G., Esper O., Lamy F., Jaccard S. L.,
Wacker L., Oleynik S., Gersonde R. and Haug G. H. (2015)
Antarctic Zone nutrient conditions during the last two glacial
cycles. *Paleoceanography* **30**, 845–862. <https://doi.org/10.1002/2014PA002745>.
- Sundermeyer-Klinger H., Meyer W., Warninghoff B. and Bock E.
(1984) Membrane-bound nitrite oxidoreductase of *Nitrobacter*:
evidence for a nitrate reductase system. *Arch. Microbiol.* **140**,
153–158.
- Talley L. D. (2013) Closure of the global overturning circulation
through the Indian, Pacific, and Southern Oceans: schematics
and transports. *Oceanography* **26**(1), 80–97.
- Vanzella A., Guerrero M. A. and Jones R. D. (1989) Effect of CO
and light on ammonium and nitrite oxidation by chemolitho-
trophic bacteria. *Mar. Ecol. Prog. Ser.* **57**, 69–76.
- Wada E. and Hattori A. (1978) Nitrogen isotope effects in the
assimilation of inorganic nitrogenous compounds by marine
diatoms. *Geomicrobiol. J.* **1**(1), 85–101.
- Wang X. T., Sigman D. M., Prokopenko M. G., Adkins J. F.,
Robinson L. F., Hines S. K., Chai J., Studer A. S., Martinez-
Garcia A., Chen T. and Haug G. H. (2017) Deep-sea coral
evidence for lower Southern Ocean nitrate concentrations
during the last ice age. *PNAS* **114**(13), 3352–3357.
- Ward B. B. (1985) Light and substrate concentration relationship
with marine ammonium assimilation and oxidation rates. *Mar.*
Chem. **16**, 301–316.
- Weigand M. A., Foriel J., Barnett B., Oleynik S. and Sigman D. M.
(2016) Updates to instrumentation and protocols for isotopic
analysis of nitrate by the denitrifier method. *Rapid Commun.*
Mass Spectrom. **30**(12), 1365–1383. <https://doi.org/10.1002/rcm.7570>.
- Wu J., Calvert S. E. and Wong C. S. (1997) Nitrogen isotope
variations in the subarctic northeast Pacific: relationships to
nitrate utilization and trophic structure. *Deep-Sea Res. I* **44**(2),
287–314.
- Wunderlich A., Meckenstock R. U. and Einsiedl F. (2013) A
mixture of nitrite-oxidizing and denitrifying microorganisms
affects the $\delta^{18}\text{O}$ of dissolved nitrate during anaerobic microbial
denitrification depending of the $\delta^{18}\text{O}$ of ambient water.
Geochim. Cosmochim. Acta **119**, 31–45.
- Zakem E. Z., Al-Haj A., Church M. J., van Dijken G. L.,
Dutkiewicz S., Foster S. Q., Fulweiler R. W., Mills M. M. and
Follows M. J. (2018) Ecological control of nitrite in the upper
ocean. *Nat. Commun.* **9**, 1206. <https://doi.org/10.1038/s41467-018-03553-w>.